UNIVERSITEIT VAN AMSTERDAM

MSc Chemistry

Science for Energy and Sustainability

Master Thesis

Investigation of singlet fission solar cells from perylene bis(phenethylimide)

---

by

Maarten Mennes
10823026

September 2016
54 ECTS
Period: October 2015 – September 2016

Examiners:
prof. dr. A. Polman
dr. E. von Hauff

Daily supervisor:
dr. Bruno Ehrler

Abstract

Singlet exciton fission is one of the ways to circumvent the Shockley-Queisser limit. This theoretical limit is 33.4% for single-junction photovoltaic devices. By only absorbing high energy photons from the spectrum and subsequently sharing this high excitation energy with one of its neighbors, certain organic molecules offer a way around this limit, and the theoretical maximum efficiency increases to 45%. Inorganic counterparts of this tandem architecture suffer from high material costs, and the organic molecules that have shown singlet fission behavior can in principle be cheap. In this work we have explored the organic semiconductor perylene bis(phenethylimide)(PDI). The incorporation of this new material into practical devices would allow for the study of singlet fission in a new material. What makes this material interesting, is that PDI has properties that makes it suitable as an electron donor. If this molecule performs singlet fission, it would be the first singlet fission molecule that has electron accepting properties, opening a way towards an all-singlet fission solar cell and thereby possibly allow to reduce thermalization losses even more. The devices that were fabricated with the PDI donor showed relatively substandard performance, reaching a J_{sc} of $0.8 mA/cm^2$ with low V_{oc}. The devices with PDI as an acceptor, in combination with a PTB7 donor, showed better performance. Specifically the V_{oc} was increased. However, although EQE experiments suggest that some of the photocurrent originates from the PDI, singlet fission was not observed during the magnetic field measurements on both photocurrent and photoluminescence (PL). More work is necessary to determine whether this PDI performs singlet fission in practical organic solar cells.

Contents

0.1 Introduction

Singlet fission is a process through which an excited chromophore can share its energy with a neighboring chromophore in the ground-state. The splitting of a S_1 state into 2 T_1 states can be efficient because the overall spinstate of the triplet pair is coupled in an overall singlet state. This process was first observed in 1965 to explain delayed PL in anthracene crystals.[73] In 1968 this theory was then used to explain the low fluorescence quantum yields observed for tetracene crystals, and in 1969 validated through magnetic field studies.[77][22] The interest in singlet fission subsided after these early years, but has recently come back due to offering a possible route to improve the efficiency of solar cells.

The anthropogenic effects of the fossil-fueled economy on our planet are not to be underestimated, and research into renewable sources of energy has burgeoned. The potential of PV technologies is large. Although the total share of PV electricity is small, the industry has shown high growth rates in the installed capacity of renewable energy technologies; in 2014 the sector noted its fastest growth rate to date with 130GW total newly installed capacity, equal to 58.5% of net additions to the global power sector. The total share of electricity generation by renewables was 22.8% in 2014. To accelerate the growth in installed capacity, the price of PV derived electricity should decrease, and efficiency of PV modules is an important factor that determines the price of the electricity. Assuming continuing efficiency gains of PV technologies that we have observed over the last years, is not sustainable on a long-run. Contrarily, the so-called Shockley-Queisser limit, a theoretical maximum achievable efficiency for PV technology, does not allow for much more improvement. The simple fact that photons with an energy lower than the bandgap are not absorbed, together with the thermalization losses of photons absorbed with an energy higher than the bandgap, already limit power of the spectrum available to semiconductors to 45% for 1.1-1.4 eV bandgap materials.[72] This limit unfortunately does not take into account that there are also losses involved in practical solar cell operation, such as resistance, contact losses and Auger recombination, where a recombination event between an electron and a hole results in the transfer of an electron from the conduction band to higher energy states. When one incorporates Auger recombination into the theoretical maximum determination for mono-crystalline silicon of an optimal thickness of $110\mu m$, the value decreases to 29.4%.[66]

PV modules exists that perform above this limit for single-junction solar cells, but these so-called tandem cells are too expensive and only used in space applications. Singlet fission offers a way around this by removing the need for a tandem architecture; simply absorbing the high energy photons and converting the singlet excitons into 2 triplet excitons, with subsequent energy/electron transfer to a low-bandgap semiconductor such as silicon, is a promising route towards cheaper electricity. However, hitherto no singlet fission layer on top of a silicon cell has been able to beat the PCE of the silicon solar cell by itself. With an optimally performing singlet fission material on top of a crystalline silicon cell the theoretical maximum efficiency jumps from 33% to 45%.[74]

Although inorganic PV technologies are dominant on the market, already in 1906 Pochettino reported that a molecule called anthracene showed photo-conductivity.[60] The potential applications of organic materials as photo-receptors were recognized in the late 1950s. Many molecules followed; in the early 1960s people discovered that many common dyes, including methylene blue, displayed semiconducting behavior.[11] Progress has been made in organic solar cell research, and nowadays this technology is capable of reaching 10% efficiency. With a record efficiency of 11.5% using a polymer with a band-gap of 1.66 eV, the organic PV (OPV) field is still far behind in power converting efficiency. The interest in OPV has subsided in re-

cent years, primarily driven by the ongoing trend of the efficiency becoming a more important cost reducer for large area PV projects, and the rapid shift of interest towards the perovskite and quantum dot materials.

Organic semiconductors can circumvent some of the issues of silicon PV, such as the energy intensity of the production process, offering a potentially less expensive, more environmentally-friendly alternative. Additionally, the properties of mechanical flexibility and possible transparency can be convenient for certain applications, although the latter implies that a part of the electromagnetic spectrum is not absorbed.

The aim of this thesis is to incorporate a new singlet fission material in a device as a donor and acceptor. Singlet fission materials have only been researched as donors, but perylene bis(phenethylimide) (PDI) has properties that suggest that it is more suitable as an electron acceptor. This would open the door to an all-singlet fission solar cell, where both the electron donor and acceptor perform singlet fission, potentially reducing the thermalization losses even more. Through an introductory chapter relevant concepts of OPV will be discussed, after which we will present the fabricated devices and the results of several experiments performed on them.

Chapter 1

Fundamentals

This chapter will provide a brief discussion on the semiconducting behavior in organic systems, the singlet fission phenomenon and a short description of the important properties of PDIs.

1.1 Basics of (organic) semiconductors

1.1.1 Inorganic semiconductors

In inorganic semiconductors such as silicon and germanium, the strong covalent coupling between the atoms in the crystal and the long range order lead to the formation of electronic bands through delocalization of atomic electronic states. The wavefunction overlap between electrons on neighboring atoms has important implications on the energy; the Pauli exclusion principle states that no 2 identical particles occupying the same space can possess equal energy, and thus in an inorganic crystal the energy levels split into discrete levels. Since the atomic density in crystalline silicon are in the order of $5 \times 10^{22} \times cm^{-3}$, this leads to a close spacing of large amounts of electronic states, and thereby bands are formed. The valence band is the highest energy band filled with electrons, and the conduction band is the band where electrons can reside when they absorb sufficient energy. The Fermi level refers to the highest occupied energy level at 0 Kelvin, and is generally found between the conduction and valence band in semiconductors. One can classify solids according to the splitting of the valence and conduction band. Metals have their Fermi levels inside the energy of the valence band, which facilitates excitation of electrons into higher states, and therefore these materials show high conductivity. The Fermi level resides above the valence band for both semiconductors and insulators. This makes it difficult to excite electrons, in the order of multiple electron volts for insulators and generally < 2 eV for semiconductors. This is illustrated in the figure 1.1.

Not many electrons have enough energy to reach the conduction band, in silicon crystals at room temperature approximately only one electron per 6.9×10^{12} silicon atoms, and this leads to low intrinsic carrier concentrations. The introduction of small amounts of foreign elements with a different valency, in the case of silicon trivalent or pentavalent elements, can be used to create an extrinsic semiconductor with higher conductivity. When one introduces a trivalent impurity, or acceptor impurity, into the pure silicon crystal, a so-called $p-type$ semiconductor is created. The element used is most often boron. Being a group 3 element, the boron readily accepts an electron from the silicon valence band into its own valence shell. The boron becomes negatively charged and the electron is left immobile due to the incorporation into the valence shell, leaving behind a hole. The use of group 5 elements, especially phosphorus, leads to the reverse process; the extra valence electron of the impurity will, at room temperature, jump to

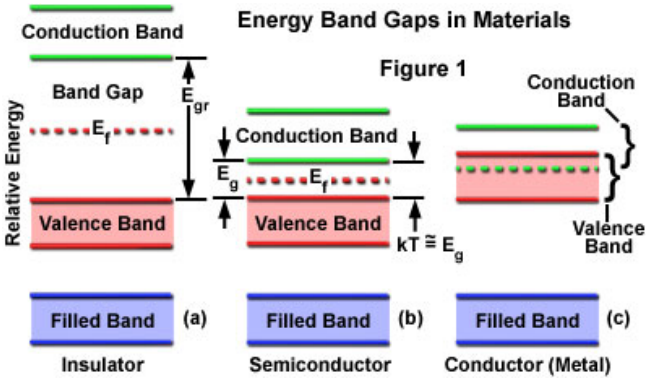

Figure 1.1: Simplified image of band structure in metals, semiconductors and insulators. Obtained from [75]

the conduction band, leaving a positively charged atom behind. The hole is left immobile and the extra electron counts towards the electron concentration. Thereby $n-type$ semiconductors are created.[71] When a $p-type$ and a $n-type$ are brought together, a so-called pn-junction forms. The pn-junction is the electronic structure which gives rise to diode behavior, and is also important in PV. The majority-carriers near the interface between the semiconductors will diffuse across the junction and recombine - a depleted region forms which is virtually free of majority carriers. The different dopants in this region are charged ions and thereby create an electric field, preventing further diffusion. Applying a forward bias, the field potential is weakened so the barrier height in the junction lowered, and therefore the resistance to current flow drops to near zero. On the other hand, applying a voltage in the opposite direction, which increases the potential barrier, is called reversed bias. The resulting field at the junction is enhanced and the barrier height now prevents flow of charge carriers across the junction. When a photon with sufficient energy is absorbed, it will excite an electron that can then freely move, leaving behind a hole. The electric field in the material will force the electron to flow to the n-type semiconductor whilst the hole will flow to the p-type material. Connecting the 2 materials via an external circuit will allow the charge carriers to do work.

Crystalline silicon is a so-called indirect bandgap material. Although the detailed explanation is beyond the scope of this thesis, it is important to point out. This justifies, to some extent, the research into organic (which are direct bandgap) semiconductors. Organic semiconductors have high absorption coefficients compared to silicon, allowing the active layers of a PV device to be relatively thin. This builds on the rule that besides energy conservation, momentum also has to be conserved during an absorption event. During the transfer of an electron between the valence band and the conduction band should occur with conservation of energy and momentum, irrespective of the band structure. In a direct band-gap semiconductor, the 2 states defining the band-gap occur at the same value of momentum, i.e. lying along the same k-vector[1]. When a photon of the band-gap energy hits a direct band-gap semiconductor an electron hole pair is produced easily. However, incident photons on an indirect band-gap semiconductor should be accompanied by the emission or absorption of a phonon, i.e. a lattice vibration. The probability of this second order process is lower, and therefore solar cells of indirect band-gap semiconductor need to be a lot thicker.[52] Only 1 micron material of the direct bandgap semiconductor gallium arsenide is needed to absorb an equivalent amount of light as 100 microns of silicon. The trade-off that arises is that in a direct band-gap semiconductor absorption coefficients are higher, but the carrier lifetimes decrease as the reverse process, i.e.

[1]k (wavevector = momentum/hbar)

recombination, is also more efficient.

The creation of the bands in inorganic semiconductors is not something that occurs similarly in organic semiconductors, where the basic unit of the crystal lattice are molecules instead of atoms. The consequences of this difference will be the focus of the next part of the thesis.

1.1.2 Organic semiconductors

The previous section dealt with the combination of atomic electronic states in inorganic crystals forming band structures, and we will now take a closer look at the characteristics of organic molecules that facilitate semiconductor behavior. This chapter will start with the description of electronic states in organic molecules. The exciton, a neutral quasi-particle underlying all photophysical properties of organic semiconductors, will then be discussed. Thereafter, electronic transitions are discussed. This chapter will end with a theoretical description of singlet exciton fission, the actual topic of this thesis, and a review of the operating principles of organic PV devices and common molecules and device architectures encountered in this field.

1.1.3 Electronic states in conjugated organic molecules

The discovery that organic molecules are brightly colored, led scientist to the realization that organic molecules can interact with the visible light region of the electromagnetic spectrum. This was found to be especially true for the conjugated organic molecules.[69] This behavior is a result of the electronic delocalisation in these materials, where electronic states spatially spread along chains of double/triple covalently-bonded carbon atoms.[39] To gain a better understanding of what underlies this electronic delocalisation, we shall briefly consider the most simple π-bonded molecule, ethylene (C2H4). The ground state electronic configuration of both the carbon atoms is $1s^2 2s^2 2p^2$, with 2 unpaired p-electrons. Atomic orbital hybridization explains the valency of carbon and the geometry; the promotion of 1 s electron into the empty pz orbital yields $1s^2 2s^1 2p^3$, to form 3 degenerate, co-planar and orthogonal orbitals. When 2 sp^2 hybridized carbons approach each other, 1 σ-bond is formed by the combination of 2 hybrid orbitals, resulting in enhanced electron density between the 2 nuclei. The binding energy of these electrons is typically in the order of 10 eV, too high to be involved in optical processes. The wavefunction of the unpaired electron left in the unhybridized p orbital is positioned perpendicular to the 3 hybrid orbitals, and can overlap with a similar orbital on the neighboring carbon atom, thereby forming a π-bond. The electrons involved in the π-bond have zero probability of residing in the plane of the sp2 orbitals, and the probability cloud extends above and below the carbon chain.[4] The schematic outline of this orbital arrangement can be seen in figure 1.2.

The repetition of sequential π-bonds, so-called conjugation, has a strong influence on the structure of the molecule due to the formed energetic barrier which prevents free rotation around the σ-bond axis. Although this determines to a large extent the structure and behavior of these molecules, the justification for our discussion here lies in the fact that the π-electrons are relatively weakly bound and can interact with photons from the visible part of the spectrum. [4] The addition of more sp^2 hybridized atomic orbitals leads to further delocalization of the molecular orbitals and narrows the gap between the highest occupied molecular orbital (HOMO) and the lowest unoccupied molecular orbital (LUMO), and these are the 2 orbitals that are involved in OPV. A simplified method to determine the energies of the molecular orbitals in conjugated molecules was first created by Erich Hückel in 1930.[33] In this method molecular

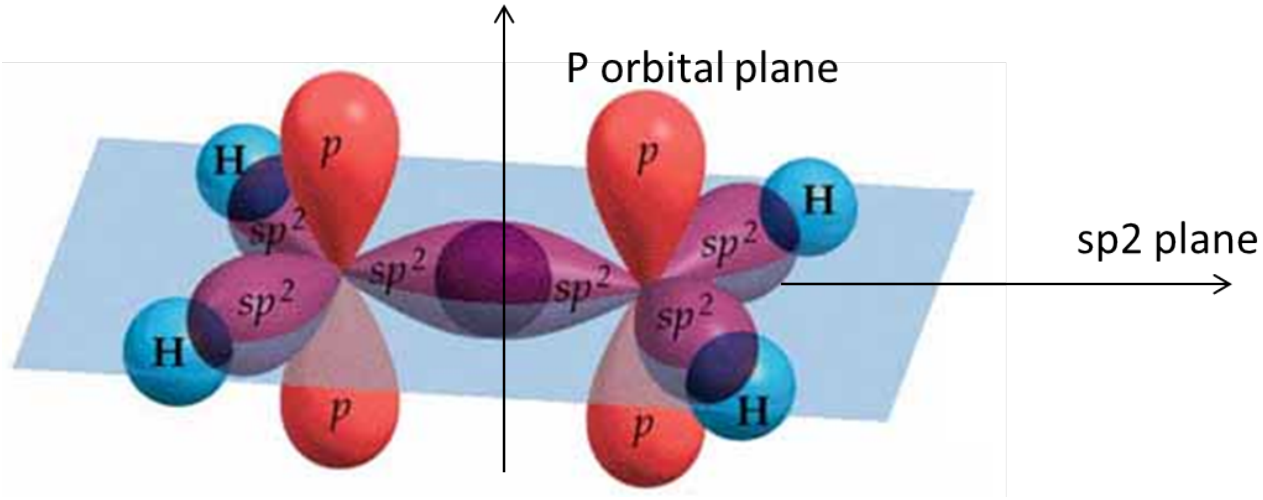

Figure 1.2: Orbital image of ethylene

orbitals (MOs) are formed as linear combinations of atomic orbitals (LCAO);

$$\psi = c_1\phi_1 + c_2\phi_2$$

where Ψ is the MO, ϕ_n are the AOs and c_n are their coefficients. To determine the coefficients one may substitute this equation into the Schrödinger equation and apply the variational principle, which is used in quantum mechanics to construct the coefficients for each atomic orbital. For a more elaborate discussion on the workout of MO energies, the reader is referred to established reference work.[30] When 2 AOs interact, 2 MOs are formed; 1 bonding MO and 1 anti-bonding MO that, when occupied, lower or raise the energy of the molecule, respectively. The MO with more nodes, i.e. points where $\Psi = 0$, is higher in energy since the energy is proportional to the second order spatial derivative of the wavefunction, and high numbers of nodes imply high curvature. As mentioned above, 2 MOs are of particular importance, the HOMO and the LUMO. The energy difference between these is the lowest optical transition that can take place, and thus this energy difference corresponds to the band-gap of the material. Their spatial extent is important for the efficiency of charge transport.[10] Before delving into the main purpose of this thesis, singlet fission, we will take a closer look at what happens when an electron is excited from the HOMO to the LUMO by an incoming photon. The properties of the resulting neutral quasi-particle, also known as the exciton, underlying most of the behavior of organic semiconductor, will be discussed next.

1.1.4 The exciton

In electromagnetism, the resistance of a certain medium to the formation an electric field is called the permittivity. The relative permittivity, also known as the dielectric constant, κ, is the ratio between the permittivity of the medium to that of the permittivity of the vacuum. Thus, the permittivity describes a medium´s ability to resist an electric field. A polar medium, containing significant amounts of polar components such as polarized covalent bonds, has a higher dielectric constant because the dipoles can reorient themselves in response to an electric field. The strong dielectric screening in most inorganic semiconductors results in Mott-Wannier excitons, and free charges can be readily formed at room temperature since the Coulombic force between the hole and the electrons are compensated. Whereas in inorganic crystal structure the basic unit of the crystal are atoms, for organic crystals these are molecules. The molecules

are bound through relatively weak intramolecular Van der Waals interactions, and excited states tend to be localized on single molecules. Organic materials therefore have significantly lower dielectric constants, resulting in strong Coulombic attractions between the electron and the hole due to inefficient screening; usually in the order of 0.5-0.9eV, thus much bigger than kT at room temperature.[62] These Frenkel excitons are the origin of much of the fascinating behavior, but also challenges, of organic semiconductors. The localization of the exciton can be observed when comparing absorption spectra of an organic semiconductor in different states, such as in solution, thin film and single crystals. The data from these experiments vindicates the notion that excited states in solid state organic semiconductors are mostly dependent on the characteristics of the single molecule.[51][1]

Electrons are fermions, having a half-integer spin, and spin physics plays an important role in the exciton. The promotion of an electron from the HOMO to the LUMO allows us to treat the excited state as a 2-electron system and 2 fermions can give rise to 4 spin states. Subsequent addition of angular momenta following the well-established rules of quantum mechanics [62]:

$$|ls = 1, m = 1 >= |\uparrow\uparrow>$$
$$|ls = 1, m = -1 >= |\downarrow\downarrow>$$
$$|ls = 1, m = 0 >= |(\uparrow\downarrow + \downarrow\uparrow)/\sqrt{2} >$$

These states have a total angular momentum of one, and are called triplet excitons. The remaining state has a total angular momentum of zero, and accordingly called a singlet:

$$|ls = 0, m = 0 >= |(\uparrow\downarrow - \downarrow\uparrow)/\sqrt{2} >$$

where the arrows correspond to either spin up or spin down, the s and the m to the eigenvalues of the total angular momentum operator and the projection of angular momentum on the conventional z axis, respectively. The above representations imply that triplet wavefunctions are symmetric under particle interchange, whereas the singlet is anti-symmetric. This has implications for the spatial wavefunction of the 2 electron system; where now the spatial wavefunction of singlet and triplets are symmetric and antisymmetric, respectively. Thus, optical transitions are only allowed between states of equal total spin, i.e. singlet $\rightarrow$ singlet, triplet $\rightarrow$ triplet etc.. Additionally, when we neglect electron-electron interactions the singlet and triplet states are degenerate, but one has to introduce an exchange interaction when considering real systems. [45] The repulsion between the 2 electrons correlates with the partial overlap of the HOMO and the LUMO. This implies that the exchange energy depends predominantly on the extent to which wavefunction amplitudes reside on the same atomic site, as further delocalization of the π system decreases the amplitude accordingly.[74] For most conjugated systems this exchange interaction lowers the triplet energy relative to the singlet energy by a couple of hundred meVs.[45] This splitting of the singlet and triplet states in conjugated systems is an essential feature which has to obey requirements in order for singlet exciton fission, the main theme of this thesis, to happen efficiently. The splitting can be much larger in the polyacene group, alternate hydrocarbons for which the Hückel method predicts large overlap between the HOMO and the LUMO.

1.2 Singlet fission

Opting for single-junction solar cells inevitably leads to significant spectral losses. Whilst photons with an energy below the bandgap energy are simply not absorbed, high energy photons

are absorbed but quickly relax down to the minimum energy of the conduction band. Singlet fission addresses this issue by absorbing high energy photons, with a subsequent spin allowed process in which an excited chromophore shares its energy with a neighboring chromophore. Upon the absorption of a photon, the first allowed energy level is the S_1. The singlet nature of the initial and final state means that this transition is spin allowed. In organic semiconductors a triplet state is sometimes available at roughly half the energy of the S_1, the so-called T_1 energy level. When a chromophore shares its singlet excitation energy with a neighboring chromophore, the S_1 state can "split" into two T_1 states, each on one molecule. The conversion of $S_1 \rightarrow T_1$ is spin-forbidden, and the low probability of such processes means it is usually kinetically out-competed. However, $(S_1 \rightarrow 2T_1)$ is a spin allowed process because the resulting triplets are coupled into an overall singlet state. The process can be very rapid because spin is conserved, as diplayed in figure 1.3. The idea of singlet fission was first put forward by Singh et al., to explain

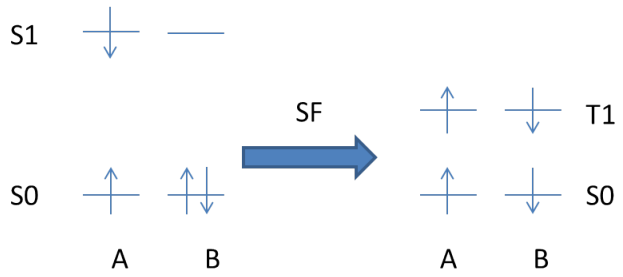

Figure 1.3: Schematic representation of singlet fission at molecules A and B

the delayed fluorescence in crystalline anthracene which seemed temperature dependent.[73] They presumed that the delayed signal came from the singlet exciton fission with subsequent triplet-triplet annihilation. In order for this effect to manifest itself in the data, the process must be efficient and kinetically out-compete other processes. This interesting theory led to a body of research in the 60s and 70s focusing on similar experiments that tried to identify singlet fission in other materials, including tetracene and pentacene crystals.[43][12] The signal corresponding to direct decay of S_1 to S_0 was referred to as prompt fluorescence, whilst the singlet fission with subsequent triplet-triplet annihilation signal was called the delayed fluorescence. It turned out that these two signals, and the ratio between them, could be changed by introducing an external magnetic field.[22][42] This discovery made it easier to detect materials that showed this effect but also allowed for the first theoretical description of the singlet exciton fission. In Johnson and Merrifield's theory the singlet is coupled to the triplets by an interacting triplet pair, and the efficiency of singlet fission depends on the coupling between the $S_0 + S_1$ state and the state of the triplet pair, which is in turn depends on the fractional character of singlet $(TT)^1$ in the triplet-pair state. The eigenstates of the triplet-pair state also include the other ways to combine two triplets, $(TT)^5$ and $(TT)^3$, and the relative presence of each is dictated by the spin hamiltonian, H_{sp}, and thereby indirectly by the strength and direction of the magnetic field through the Zeeman term (oversimplification but valid in single crystals).[22] [53] The transition from the S_1 state to a triplet state is also the result of a process called intersystem crossing, as discussed previously. In the studied molecules there were no heavy atoms present that could speed up the intersystem crossing rate through spin-orbit coupling, and a clear distinction was made because the singlet fission process is rapid in these molecules nonetheless.[54] By the coupling of 2 triplet states in an anti-parallel way, the process conserves angular momentum. Once created, the 2 triplet excitons can diffuse apart, and the following scheme fully covers the process;

$$S_1 + S_0 \rightarrow (TT)^1 \rightarrow T_1 + T_1$$

where the $(TT)^1$ is the coupled triplet pair. For simplicity here the initial state is the first excited singlet state, but this can be higher singlet states as well. The singlet fission process here is represented by a 2 step mechanism with an intermediate coupled state, but there has not been conclusive evidence whether this is a real state or merely a virtual intermediate.[74] A reason for breaking the process up into 2 parts is to explain the magnetic field dependence. In 1970, seminal work by Merrifield and Johnson, described the recombination of free triplet excitons, considering competing decay channels for the $(TT)^1$ intermediate. From here it can either go back to the singlet state, which results in a decreased delayed fluorescence signal, or it can combine with other triplet-pair states. When the latter process occurs, eventually the state will split into free triplets and lead to delayed fluorescence through triplet-triplet annihilation.[74] We will now dive a little deeper into the basic physics behind singlet fission.

1.2.1 Theory of singlet fission

As discussed above, and becomes apparent from the diagram, 2 possible routes exist towards the triplet states; a direct pathway and a charge transfer mediated pathway. It is assumed that the photoexcitation is localized on an individual chromophore and due to electronic coupling spreads to a state residing on both the chromophores and this ultimately leads to 2 triplet states on neighboring molecule. A recent study by Greyson et al., considers a 4 electron system in 4 orbitals, giving rise to 70 different configurations.[26] Out of these 70 electronic configurations, merely the S_1S_0, S_0S_1, T_1T_1 are interesting for the purpose of investigating singlet fission. This is represented in the diagram in figure 1.4. Both the direct and indirect pathway may be

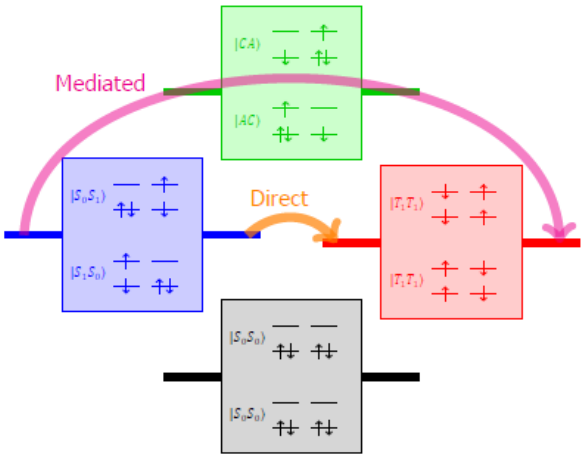

Figure 1.4: Schematic diagram of the singlet fission process

important, depending on the electronic coupling and the energetics of a particular system, and evidence for both has been presented. Although in many cases the charge transfer state is treated as a virtual intermediate, one cannot disregard this state as the electronic coupling matrix elements for the mediated process are larger than for the one step process. In a more recent approach by Berkelbach et al., an attempt was made to draw a microscopic picture of singlet fission in dimers.[6] Taking a Redfield approach they described the dynamics of electronic states through phonon coupling. A detailed description of this work is beyond the scope of our present discussion, and the interested reader is referred to [6]. The $(TT)^1$ state is a the so-called correlated triplet pair, and this "pure" singlet state is a superposition of the wavefunctions of the nine sublevels that arise from combining two triplets which are not pure spin states. It

must be noted that the representation here is an oversimplification, and are more properly described by the Johnson-Merrifield model. The 2 chromophores, where the 2 triplet excitons reside, are described by Hamiltonians, which contain a part that deals with their interaction as well as a part that describes the individual chromophore in the absence of any interaction. The total Hamiltonian for a triplet pair in a crystal lattice is assumed to be the average of the two individual triplet excitons, which are described by the spin Hamiltonian;

$$H_{spin} = g\beta B \cdot S + D(S_z^2 - \frac{1}{3}S^2) + E(S_x^2 - S_y^2)$$

where g is the g-factor, β the Bohr magneton, B the magnetic field, S the total spin operator, $S_{x,y,z}$ the operators along the axes, and D and E the zero field splitting parameters. The nuclear segment of the Hamiltonian is assumed irrelevant due to fast electronic motion.
Starting with the S_0+S_1, the interaction Hamiltonian is allowed to generate the final diabatic[2] T_1+T_1 state, which are eigenstates of the individual chromophores. The interaction Hamiltonian is usually divided into the spin dependent part and the electrostatic part. The electrostatic Hamiltonian describes the attraction between nuclei and electrons, the mutual repulsion between nuclei and electrons, and the kinetic energy of electrons. This part of the interaction Hamiltonian is responsible for turning the two singlet states into the coupled triplet. The spin Hamiltonian, on the other hand, contains operators of spin dipole-dipole interaction, the interaction with a magnetic field and spin-orbit coupling. The spin Hamiltonian can mix states of different spin multiplicity, and is therefore said to be involved predominantly in the intersystem crossing part of singlet fission, i.e. the decoupling of the two triplet states into free triplets. The presence of an outside magnetic field affects the spin Hamiltonian and the rate of singlet fission can be influenced due to the presence of the Zeeman terms. The transition S_0+$S_1 \rightarrow T_1$+T_1 comprises a transition between diabatic potential energy surfaces, something that could proceed via conical intersections. The vibrational coherence in the excited singlet state is transferred to the triplet states, and strongly resembles ultrafast internal conversion. This suggest that singlet fission and internal conversion are mediated by similar relaxation processes, through the coupling of nuclear and electronic vibrations. The two potential energy surfaces can become degenerate and the Born-Oppenheimer approximation breaks down. In a study using TIPS-pentacene, the photo-excitation of certain modes shuttle the exciton to the region where the S_1 and the $(TT)^1$ potential energy surfaces are degenerate due to vibronic coupling. This suggests that a general theory of singlet fission should account for nuclear degrees of freedom.[57] We note here once more that regarding singlet fission as a two step process is just a convenience, and a universal mechanism for singlet fission has not yet been established.

1.2.2 Singlet fission candidates

The transition from S_0+S_1 to $(TT)^1$, like most other molecular processes, often only proceeds when a certain activation energy is provided. This energy can not be too high because when the rate becomes too slow, the relatively short-lived S_1 state will take the fluorescence route. The S_1 state can also undergo singlet fission before vibrational thermal equilibrium has been reached, for instance when higher lying singlet states become populated by light absorption. In this case singlet fission competes with internal conversion processes, which usually occurs rapidly and thereby out-competes singlet fission. As a starting point, one often does well to pick a molecule with a near unity quantum yield for fluorescence, meaning that the singlet fission

[2]Rapidly changing conditions effectively prevent the system to adapt to the changes during the process, and the spatial probability density remains unchanged

competing process intersystem crossing is not significant. This unfortunately does not mean that in an organic crystal the inter-molecular processes do not compete with singlet fission. The value of the $E(2T_1) - E(S_1)$ is often a positive number, which means that singlet fission is an endoergic process and singlet fission will not occur efficiently when this value rises far above k_BT. In some molecular systems, such as tetracene, the triplet energy can be more than half of the singlet and singlet fission uses temperature dependent phonon modes from the environment.[27] Recent reports suggest that the the entropic gain from the evolution of 1 particle (singlet) into 2 particles (2 triplets) could be a factor that promotes singlet fission, similar to the entropic gain due to exciton dissociation at donor/acceptor interfaces.[13][15] Another thing to keep in mind when considering singlet fission materials is the energy level of the T_2 state. When 2 T_1 states meet, which can happen due to the long lifetime of this state, triplet-triplet annihilation can occur. The result of such an event can be a singlet, triplet and quintet state. In most cases the formation of a quintet state is too endoergic, but when it does occur the quintet state still possesses two excitations which can result in free charge carriers. On the other hand the formation of an S_0 and a T_1 will be too exoergic to be efficient. However, S_0 and T_2 can in certain molecules be of more concern, it is therefore important that $2 \cdot E_{T_1}$ is not closely positioned above to the energy of T_2. Additionally, it is important target molecules should have high absorption cross-sections.

Why we need new singlet fission molecules that are stable in air and light

The triplet excitons resulting from singlet fission can produce twice the current with respect to 1 S_1 exciton, but cut the photovoltage roughly in half leaving no net gain in energy. In order to increase the PCEs of solar cells, a singlet fission material must be combined with another material that absorbs low energy photons. A singlet fission layer which absorbs the high-energy photons, positioned on top of a normal semiconductor which absorbs the low energy photons can be a worthwhile endeavor; Shockley-Queisser calculations predict a maximum efficiency to increase from 33.4% to approximately 45%.[74] The photons with an energy below the singlet fission material bandgap, but above the bandgap edge of the low-energy photon absorbing semiconductor, will still lose their energy non-radiatively.

The most common molecule in the singlet fission field is pentacene. Although singlet fission is very efficient in pentacene, it has several disadvantages; pentacene is vulnerable to degradation caused by incident light and also degrades when exposed to air via the formation of a transannular peroxides and dimeric peroxides.[7] This form of degradation will deteriorate the charge transport properties and the absorption, leading to large drops in generated photocurrent. Susceptibility to photo-oxidation is a property that is highly undesirable for materials that find their application in PV, and therefore the need exists to research singlet fission materials that are more stable than pentacene. PDIs have been used for many years as industrial pigments and dyes as they are relatively resistant to thermal/photo-chemical/oxidative degradation. The current work will investigate a PDI derivative that is reasonably stable in air and light and in theory should perform singlet fission with 190% efficiency. The molecular structure can be seen in figure 1.5.

Proving singlet fission as origin of photocurrent

Singlet fission is being studied extensively and in order to prove that singlet fission is actually the origin of the photo-current in a solar cell, certain experiments are used. An experimental difficulty of singlet fission research is the detection of the phenomenon, in part due to the need to distinguish between triplet formation following singlet fission and triplet formation

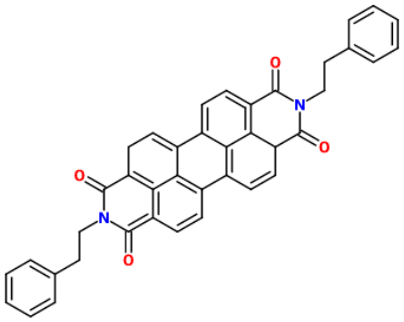

Figure 1.5: Molecular structure of perylene bis(phenethylimide)

resulting from intersystem crossing via spin-orbit coupling. A quantum efficiency exceeding 100% is conclusive evidence for singlet fission. This is difficult to achieve, but was recently shown in a study by Congreve et al..[16] A more popular method is to probe the magnetic field dependence of the photocurrent. According to Johnson and Merrifield's theory the singlet character initially increases slightly with the B-field before falling, and indeed this is often observed in magnetic photocurrent studies of singlet fission devices.[53] Another way to exploit magnetic field dependence is to perform PL experiments under magnetic fields, and analyze the yield of prompt- and delayed fluorescence.[23] As the magnetic field increases to above 0.2 Tesla, the Zeeman interaction term will start to dominate the spin Hamiltonian and hence the singlet character of the $(TT)^1$ state decreases, and the singlet fission rate will fall with it.[8][62]

Generally, the ways of studying singlet fission experimentally can be divided in electrical and optical viewpoints. The optical methods include transient absorption, time resolved PL studies and photoelectron spectroscopy. Back in the 1960s and 1970s singlet fission was studied using the time dependence of PL. As previously stated the delayed component in the signal from anthracene and tetracene was ascribed to singlet fission.[73] The signal arises due to triplet-triplet-annihilation, as phosphorescence should be very inefficient in the those organic molecules. It must be noted that this method of studying singlet fission requires the singlet fission process to not be too exoergic, as triplet-triplet-annihilation will not happen if the triplet level is positioned significantly below half that of the S_1. Time resolved absorption measurements for the study of singlet fission is much more common nowadays, as the the triplets can be detected directly. Ground state bleach concurrent with decay of the excited singlet state and triplet formation on an ultra-fast timescale (sub-nanosecond) indicates of singlet fission.[37] These time resolved techniques are difficult to analyze because signals often overlap to a large extent, so not all groups do this. At high intensities, the triplet-triplet annihilation leads to increased emissions, complicating results and this requires one to have extensive information regarding the energy levels in a material.[28] One can exploit this characteristic by doing the femto-second transient absoprtion experiments.[20][56][46] The origin of data points can be relatively safely ascribed to singlet fission as long as there are no heavy atoms in most systems, since this will usually slow down regular intersystem crossing to $>$ 10 picosecond. It must be noted that, depending on the singlet fission material being researched, the timescale of singlet fission can sometimes exceed 25 picoseconds.[61] In the materials where $2E(T) > E(S_1)$, and singlet fission is thus endoergic, the triplet formation depends on the temperature of the system. This allows one to probe the ratio between prompt and delayed fluorescence, magnetic field response, triplet absorption and singlet lifetime as a function of temperature.[79] [78] Unfortunately intersystem crossing is, in certain cases, also temperature dependent, and therefore cannot by itself be regarded as evidence for singlet fission.[50]

1.3 Photophysical processes

This section of the thesis will start with a description of the absorption process in an organic molecule. Subsequently we will describe the processes that can happen after the absorption, and thus compete with singlet fission.

1.3.1 Optical transitions

When Maxwell summarized the classical ideas in his *Electromagnetic Theory*, light was treated as two propagating waves of a magnetic and an electric field. The time-dependent expression for this electric field, most relevant to our discussion here, is, in one direction:

$$E(x,t) = E_0(x)[e^{i\omega t} + e^{-i\omega t}]$$

where ω is the angular frequency of the radiation and E_0 is the maximum amplitude of the field in the direction of x.[24] The energy of of electromagnetic radiation varies between γ-rays (10^7 eV) and radio waves (10^{-9} eV). The energy of these waves is carried by photons and when the energy of photons matches the energy difference of available states in a material, the photons can be absorbed:

$$\delta E(E_2 - E_1) = \hbar\omega$$

At room temperature the majority of the molecules are in the ground state, and the populations are dictated by the Boltzmann factor. Assuming a ground state of singlet character, S_0, and another higher lying singlet state, S_1, the wavefunctions we denote ψ and $\bar{\psi}$, respectively. The interaction of photons with organic semiconductors relies on the transition dipole moment:

$$\mu|f \leftarrow i|$$

where a transition takes place between the initial state i and final state f. In the well known Fermi ´s Golden Rule, the transition from one eigenstate to a continuous batch of other energy eigenstates affected by a perturbation is described in simple terms. Introducing the perturbation of the transition to the Hamiltonian of the initial state, allows one to express a system in terms of a system of which the mathematical solution is known. The initial state i and the final state f are assumed to be eigenstates of the unperturbed Hamiltonian, and the inclusion of the time dependent interaction Hamiltonian, $H_i(t)$, allows the eigenfunctions of the complete time-dependent Hamiltonian to be expressed as an expansion over the unperturbed states. The total energy of the molecule, described by the Hamiltonian operator, in the presence of an electric field is thus described by:

$$\bar{H} = \bar{H}^0 + (\mu \cdot E)$$

where the initial Hamiltonian operator is $\bar{H}^0$, and μ is the dipole moment operator. The perturbation creates a time dependent superposition of the two wavefunctions resulting in overlap between the orbitals. The electron can now oscillate between the two orbitals. The transition dipole moment is the dipole moment associated with the redistribution of electrons in a molecule during an emission or absorption. A large transition dipole moment means that there will be a strong interaction between the molecule and the electric field, resulting in a large displacement of the electrons from their initial ground state position. Similar to an oscillating dipole this then generates a transition dipole moment, determining the strength of the transition. Through this interaction the molecule gains energy of the radiation by promoting an

electron to a higher energy level. The absorbed energy is emitted when the electron recombines, and this can happen radiatively and non-radiatively, where a photon and a phonon are emitted, respectively.
The Schrödinger equation does not always have an analytic solution. However, since electrons are only a fraction of the weight of a nuclei, electrons respond nearly instantaneously to nuclear movement. This allows one to solve the Schrödinger equation for electrons in static electric potential by assuming a fixed nuclear position. This so-called Born-Oppenheimer approximation is used in the Franck-Condon principle, which explains optical behavior and absorption/emission spectra for molecules. The Franck-Condon principle is used to describe vibronic transitions, characterized by simultaneous electronic and nuclear vibrational transitions. A photo-excitation transforms the nuclear configuration by a Coulombic force resulting from a redistribution of electrons, and, as described by the Born-Oppenheimer approximation, the nuclear framework is stationary during the electronic transition. Because the configuration coordinate should not change during the electronic transition, the transition occurs between vibrational states that maximize overlap of the wavefunctions.

1.3.2 Intersystem crossing

The photophysical properties are strongly affected by the spin of the electrons; when the ground state has singlet character, with 2 electrons paired with antiparallel spin, a triplet exciton is quantum mechanically forbidden to radiatively decay back to ground state. Instead this can only happen when the singlet and triplet states mix through spin-orbit coupling, and the process is called intersystem crossing, referring to transitions between electronic states of different spin manifolds. The mathematical demonstration of this requirement is beyond the scope of the present discussion, but builds on the electric dipole matrix element between pure spin-states with different spin being zero. Spin-orbit coupling can be understood intuitively by the rotation of the electron around its own axis and the concurrent rotation around the nucleus. Both of these processes create magnetic moments and the spin-orbit coupling is a result of the interaction of these two magnets. In quantum mechanics angular momentum coupling is the procedure of the construction of eigenstates of angular momentum from eigenstates of separate angular momenta, and in the case of spin-orbit coupling the relevant interaction is between the orbit and the spin of particles where a weak magnetic interaction between the orbital motion of a particle and its spin have several implication for the photophysical properties. The most notable effect is the partial relaxation of the selection rules by compensating a change in spin angular momentum with a concurrent change in orbital angular momentum.[44] The decay of a resulting triplet state to the singlet ground state is denoted as phosphorescence, and is several orders of magnitude slower than decay channels of quantum mechanically allowed transitions. Although it is an important process in organic photophysics, the process is rendered rather weak in most organic molecules as the interaction mechanisms scales to the 4^{th} power with the atomic number, meaning that it is far stronger in molecules with heavy atoms present.[5] As already mentioned the timescales of intersystem crossing are much longer, meaning that triplet excitons have significantly longer lifetimes. This has been confirmed and the triplet lifetime is usually in the order of μ-seconds, whereas the singlet exciton lifetime is in order of hundreds of picoseconds to 10 nanoseconds.[44] The rate of intersystem crossing in the presence of spin-orbit coupling is proportional to the vibrational overlap between triplet and singlet states, as this term depends exponentially on the energy difference between them, via:

$$k_{intersystemcrossing} \propto \exp[(-(\gamma)E_d)/(\hbar\omega)$$

where E_d is the energy difference between the initial and final state and γ and ω take care of the molecular parameters and frequency of high energy phonons coupled to the π system, respectively. Intersystem crossing can be described by Fermi's Golden rule via;

$$k_{ISC} = \frac{2\pi}{\hbar}|V_{SO}|^2 \cdot \rho \cdot FC$$

where FC is the $|V_{SO}|$ is the coupling term of the spin-orbit coupling, and thus depends on the energy gap between the states via the density of states, ρ, which does not include a Franck-Condon factor, FC. The implications of this dependence on the energy difference are such that intersystem crossing is not an important decay channel between the S_1 and T_1 states, given the energy difference between them in most π-conjugated molecules. However, in some organic systems intersystem crossing can be a significant decay channel of the T_1 state to the ground state, S_0.

1.3.3 Internal conversion

Another photophysical process important for the present discussion is internal conversion, which is radiationless decay to other electronic states within the same spin group.[9] The term radiationless implies that no photons are emitted, and the dissipation of energy occurs via molecular vibrations.[44] Internal conversion is often separated in two distinct steps; first the electronic state transforms some of its energy into vibrational energy, resulting in a vibrationally excited, lower-lying electronic state. Subsequent relaxation to the lowest vibrational state occurs via the emission of multiple phonons along the potential energy surface of high energy modes.[44] This latter process is a very fast process, and thus the step limiting internal conversion is the transformation of some of the energy into vibrational energy.[21] Where in radiative transitions the initial and final states are mixed by the dipole moment operator at fixed nuclear geometry, using the Franck Condon principle, internal conversion is characterized by the mixing of states via a nuclear displacement operator at equal energy. The subsequent vibrational relaxation makes the process downhill energetic process. The vibrational state crossing rate can be described by Fermis golden rule. For internal conversion:

$$k_{ic} = \frac{2\pi}{\hbar}|V_{ic}|^2 \cdot \rho \cdot FC$$

where FC is the Franck Condon factor which is not included in the density of states, ρ, and the coupling element V_{ic}. As the density of states with the energy gap between the involved states and with molecular parameters such as number of atoms, this leads to the conclusion that internal conversion is the dominant relaxation process for higher electronically excited states, and for the S_1 state this does not necessarily hold. The inverse exponential correlation with the energy difference between vibrational levels also implies that molecules with a low lying S_1 state will have high radiative constants. The V_{ic} will be larger for states close together in energy. This can go to such extremes that so-called conical intersections are formed. Recently the involvement of conical intersections in singlet exciton fissions was explored, and it seems that at these intersection radiationless decay between states of very different energies can occur.[57] When potential energy surfaces of different electronic states intersect, the Born-Oppenheimer approximation breaks down and rapid conversion of electronic energy to vibrational energy is allowed thereby facilitating fast internal conversion. [14] In conjugated organic molecules, the important molecular class in the current discussion, the density of electronic and vibrational excited states is high and therefore internal conversion can occur on timescales in the order

of 100 femtoseconds, significantly outcompeting radiative decay in these systems.[21] However, nonradiative decay from the singlet excited state, S_1, down to the ground state, S_0, is much slower due to the relatively high energy difference. The above-mentioned density of states in conjugated molecules implies that PL is generally only observed via $S_1 \rightarrow S_0$, as relaxation down to the S_1 level occur rapidly nonradiatively, this behavior was described by Micheal Kasha and hence is referred to as Kasha's rule.[40]

The Jablonski diagram in figure 1.6 shows the various processes that can occur following the absorption of a photon by a fluorophore. The grey lines represent some of the vibrational energy levels of the electronic states.

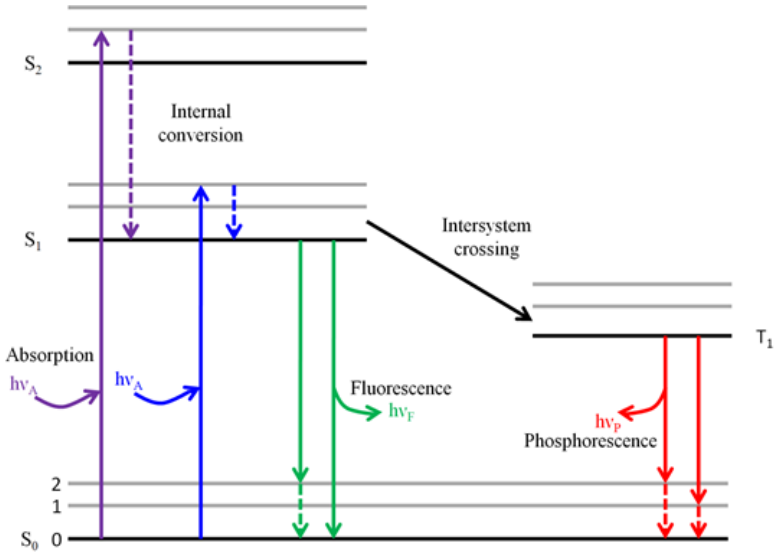

Figure 1.6: Jablonski diagram

1.4 Perylene diimides as a singlet fission material

The main driver for organic PVs has been the potential low cost fabrication, and the long term dream to successfully incorporate singlet fission materials into existing inorganic solar cells to improve the performance, whilst only minimally increase the price of the generated power. There are relatively few materials that show singlet fission, and due to the small scale production the materials are often expensive.[74]. Recent reports have highlighted the ability of perylene diimide derivatives, to be more specific perylene-3,4,9,10-tetracarboxylic acid diimide derivatives, to perform singlet fission.[18][36][64] Ford and Kamat have performed theoretical calculations on PDI in solution and determined that the first triplet state, T_1, is positioned roughly halfway between the S_0 and the S_1, indicating that the energetic constraint of singlet fission might be satisfied.[19] Perylene diimides are synthesized on a large scale and have been traditionally used as industrial dyes and pigments, having a red/purple color, and have the potential to be produced relatively cheaply. Their use as dyes and pigments showcase their outstanding photochemical and thermal stability, both desirable properties in PV applications. As will be discussed, the crystal packing geometry is of crucial importance for singlet fission and not all perylene-3,4,9,10-tetracarboxylic acid diimide derivatives share the proper geometry.[32] First the preparation of the PDI will be discussed briefly, and subsequently the electronic properties and singlet fission behavior.

1.4.1 Chemistry of PDIs

In both research and industrial processes, the starting material in the synthesis of PDI derivatives is PTCDA. The reactions of PTCDA and an aniline or alkyl amine under proper conditions results in the high yield conversion into PDI.[34] The PTCDA is obtained by the oxidation of acenaphthene followed by treatment with ammonia to give naphthalene-1,8-dicarboxylic acid imide, and the oxidative coupling of two of these molecules results in the formation of perylene-3,4,9,10-tetracarboxylic diimide, or PTCDI. To arrive at PDI, the PTCDI is first treated with sulfuric acid at 200 °C, and the resulting PTCDA is treated with an alkyl amine or aniline to give PDI. In the pigment industry, where non-soluble symmetrical PDI derivatives are the desired product, the yield can surpass 90%.[32] Ideally, in the case of PV applications, the PDI produced are soluble PDI derivatives. The synthetic routes to more soluble PDI derivatives started to appear in the 1990s, when Langhals and collegues introduced soluble moeities at the imide positions.[47] The introduction of bulky alkyl groups on these position are forced out of the PDI plane and this effectively prevents $\pi - \pi$ stacking.[32] Most derivatives with these solubilizing groups are soluble in halogenated solvents, most often encountered are dichloromethane and chlorobenzene. The soluble N, N-substituted PDIs can, in many cases, be synthesized from PTCDA with a zinc acetate catalyst above $160°C$, and usually reach 95% yield, with subsequent easy purification.[58] [47]

1.4.2 Physical and electronic properties of PDIs

The electronic properties are more relevant to the current discussion of PDIs, and these will be discussed now.

Electronic transition of N, N alkyl/aryl substituted PDIs, thus absent of any other substitutions, are observed with maxima around 525nm with molar absorptivities of roughly $10^5 M^{-1} cm^{-1}$. The PL quantum yields in these molecules approach unity, and in common solvents such as toluene the singlet lifetimes are around 4 nanoseconds.[58][84][47][48] Calculations following Intermediate Neglect of Differential Overlap (INDO) protocol have confirmed that the $S_0 \rightarrow S_1$ transition can be treated as the $HOMO \rightarrow LUMO$ transition, and DFT calculations suggest that the optical transition is polarized along the N, N-axis.[67] [41] The nitrogen atoms of the perylene core correspond to the nodal planes of the HOMO and LUMO orbitals, suggesting that substitutions here do not influence the optical properties significantly. This was experimentally confirmed when shifts smaller than 5 nanometers in both absorption and emission peaks were observed with varying alkyl or aryl groups on the N, N positions.[58] In contrast to N, N-substitutions, PDI core substitutions significantly affect optical properties; specifically the introduction of $\pi - donor$ moeities, destabilize the $HOMO$ whereas $\pi - acceptors$ stabilize the $LUMO$.[3]. This effect can be observed by significant color changes when introducing substitutions on the PDI core, with the effects increasing with their positions on the spectrochemical series. I will not further discuss the effects of core substitutions as the molecule of interest in this thesis does not contain such modifications, merely N, N-substitutions.

The relatively high electron affinity, estimated around -4 eV for simple N, N alkyl/aryl substituted PDIs, make this class of molecules interesting for electronic applications.[38] This suggests that PDIs could be electron acceptors with high electron mobilities due to high degree of $\pi - \pi$ stacking. In combination with proper molecular donors PDIs bulk heterojunction solar cells with efficiencies exceeding 7% have been fabricated.[49] Moreover, in comparison with the archetypal fullerene acceptors, PDIs are more readily tuned chemically, and exhibit strong absorption in the visible region.[35] Vacuum deposition has traditionally been the method of choice in bilayer devices, and optimized nowadays reach over 2%.[59] The wet deposition

involved in the fabrication of BHJs has been troubled by the formation of PDI aggregates in the film, leading to sub-optimal exciton dissociation, but the use of certain solvent additives can prevent this to some extent, enabling the high efficiencies seen nowadays. In these type of devices both the donor and acceptor molecules contribute to the photocurrent.[76] In these type of devices both the donor and acceptor molecules contribute to the photocurrent, which is the main difference to C60 OPV devices.[76]

As previously mentioned, PDI derivatives have properties that suggest they could be attractive fullerene alternatives as electron acceptors. In recent years several studies have appeared where PDI derivatives were used as electron acceptors, but the efficiency are still well behind the fullerene solar cells. PDI derivatives have been shown to crystallize in blends with polymers, and this leads to large scale phase separation and mixing solvents are often required.[17] Apart from the phase separation, relaxation of excitons into immobile, intermolecular states is a significant loss mechanism. These stabilized states create red-shifted emission and are formed within 100 picoseconds of photoexcitation. However, when the film is more finely dispersed, the devices are often limited by fast bimolecular charge recombination.[31] In a study by Howard et al. the intermolecular states were identified as terminal loss mechanism using transient absorption measurements. They were also able to deduce that a 20% loss in IQE was due to fast bimolecular recombination, using light intensity dependent photocurrent studies.[31] The intermolecular states are a result of the packing of the PDI, and disruption of this by addition of certain molecular groups to the nitrogen atoms of the PDI core might prove beneficial.

1.4.3 Solid state structuring of PDIs

In order to have control over the coloring properties of PDI dyes and pigments, the solid state packing behavior of PDIs has to be understood. Research started in the 1980s and it has since been revealed that the molecules for π-stacks with the PDI core parallel at a distance of roughly $3.4\mathring{A}$.[84][70][29] Substitution at the N, N positions influence the crystal packing significantly, changing both the longitudinal and transverse displacements of the molecules relative to one another. The resulting alterations in intermolecular interactions and the $\pi-systems$ change the optical properties and therefore the colors of solid PDIs vary from red to almost black.[87] As one would expect substitution at the PDI core positions can distort the π-stacking to a significant degree. Orbital overlap between molecules is a requirement for charge-carrier mobilities, and thus will partly determine the electronic properties of PDIs.

As singlet fission occurs between neighboring chromophores, the distance between nearest neighbors is likely to affect the rates of this process. Previous theoretical and experimental study showed that for two of the main classes of singlet fission molecules, the polyacenes and the biphenyl benzoisofurans, the rate of singlet fission exhibits a strong dependence on the intermolecular interaction.[68][80] In figure 1.7 the results from crystallization experiments on the PDIs are displayed, together with the displacements along both the long and the short axis. As noted previously, N, N-substitutions substitutions do not influence the optical properties much. However, they do influence the crystal packing parameters, which, in turn, affects the singlet fission efficiency. Due to steric strain the monomers become rotated with respect to each other when bulky groups are attached to the perylene. This reduces the wavefunction overlap that should exist along the N, N-axis, and will probably not exhibit singlet fission.

In figure 1.8 the time resolved PL decay profiles for multiple PDI derivatives is displayed. The top graph shows the decay profile for molecule 1, which is perylene bis(phenethylimide), in solution, and the lower graphs show all the decay profiles in thin film samples. The other PDI molecules consisted of several N, N-substituted perylene diimides, but are not a focus of the

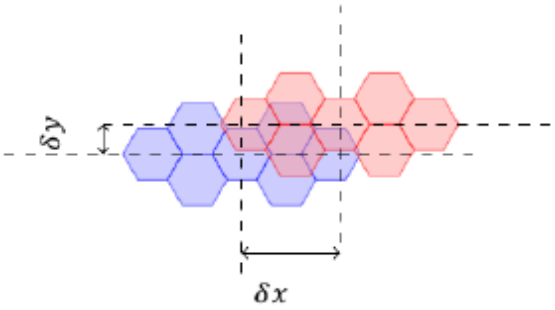

molecule	δx, Å	δy, Å
PDI **1**	3.2	0.39

Figure 1.7: Crystal packing behavior of perylene bis(phenethylimide)

current work. The horizontal axis indicates that the thin film decay profiles are much quicker, especially in perylene bis(phenethylimide), suggesting the presence of a ultra-fast non-radiative competing process.

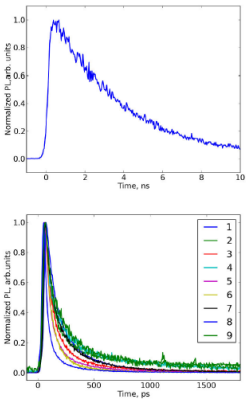

molecule	δx, Å	δy, Å
PDI **1**	3.2	0.39
PDI **4**	1.34	2.51
PDI **5**	2.48	0.02
PDI **6**	2.46	0.0
PDI **8**	3.06	1.26

Figure 1.8: Time resolved photolumiscence decay profiles of different PDIs (left), and displacement along the two axes of the PDIs (right)

1.5 Perylene bis(phenethyldiimide)

The PDI derivative of special interest in the present discussion is perylene bis(phenethylimide), displayed in figure 1.9. It has some interesting characteristics additional to the ones discussed above which make it worthwhile to investigate in organic electronics. The molecular structure, and in particular its solid-state packing behavior seems to facilitate singlet fission to occur efficiently on sub-picosecond timescales. The primary requirement for this process to occur efficiently is that twice the energy of the triplet cannot surpass the singlet excited energy by too much, i.e. $2 \times E(T)_1 \leq E(S)_1$. The rate of the 2 pathways depend on the electronic coupling between the chromophores; for the one-step process a two-electron coupling, and for the two-step process one electron couplings terms must be included. The terms that dictate the rates are determined by the orientation and distance in the crystal.[55][65] Additionally, the rate and yield of the process depends on the rates of competing processes. The fact that the singlet fission rate is so crucially dependent on the crystal packing structure allows one

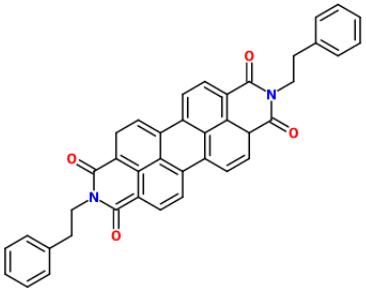

Figure 1.9: Molecular structure of perylene bis(phenethylimide)

to study the effect of chemical modifications that leave the electronic structure untouched but significantly affect the crystal packing structure.[81][82] As PDI derivatives have been used in industry for a long time, crystal structures of many derivatives are known. Theoretical calculations have identified optimal geometries for singlet fission to occur, both via the one-step- and two-step mechanism; slip-stacked geometry should facilitate highest singlet fission rates.[55][65] The optimal displacement differs with whether a one-step or two-step pathway is assumed.

The N,N-bis(phenylethyl)-PDI was subjected to extensive singlet fission experiments, including transient absorption measurements, PL studies and theoretical calculations. As this is the molecule used in the fabrication of singlet fission solar cells, the results will be discussed now. All presented data is obtained from [2].

1.5.1 Theoretical calculations

Considering a dimer of closest neighbors, the singlet fission dynamics were studied using Redfield density matrix description, similarly to other singlet fission studies on molecules such as pantacene.[63][6] The energies of the S_1 and T_1 states were calculated using time dependent density functional theory. The energetic requirement for singlet fission appears to be met, and the CT was estimated using more detailed calculations that incorporate polarization of the the environment. For a more complete explanation regarding the theoretical calculations the reader is referred to [25], the energies of the states were determined as following;

1. $E(S_0S_1) = 2.03eV$
2. $E(CT) = 3.1eV$
3. $E(T_1T_1) = 1.72eV$

From the calculations it became clear that the two-electron coupling term is much smaller than the one-electron coupling terms, suggesting that, disregarding the energy of the CT-state to be significantly higher, the direct process won't play a large role in the singlet fission process. The singlet fission in the PDI was determined to be 10.6 per picosecond. The fast rate deems other competing processes insignificant and these were not included in the calculations, and high yields are assumed.

1.5.2 Time resolved PL and transient absorption measurements

Time-resolved PL studies showed that the decay of PL is relatively quick in thin film compared to the PDI in solution. This suggest that there are processes at play which shorten the excited

state lifetime. In figure 1.10 the data by Aulin (TU Delft) is displayed. The top graph presents the time resolved PL decay profile of the monomers in solution, and the lower graph presents the same data for thin films prepared by thermal evaporation. Normalized decay profiles integrated over the emission band following an excitation at 450 nm, show a clear shortening of excited state lifetimes. The time scale suggest that there are some very fast non-radiative processes are at play in the thin film samples, and singlet fission is a likely candidate. Subsequent transient

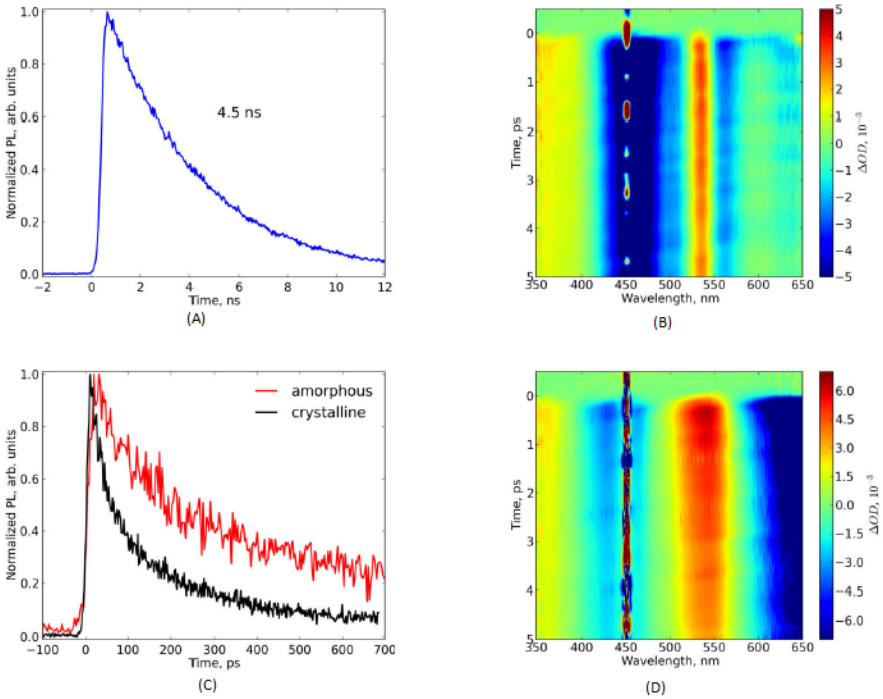

Figure 1.10: Time resolved PL decay profile (A,C), and transient absorption data (B,D)

absorption measurements shed more light on the processes going on once the PDI is excited. A clear triplet-triplet absorption feature was observed around 535 for amorphous PDI and around 540 for crystalline, and was already present at 200 femtoseconds post excitation, which is roughly the time-resolution of the apparatus. This feature corresponds to the triplet-triplet absorption observed in PDI by Ford and Kamat.[19] The appearance of this feature cannot be explained by regular intersystem crossing as it is much slower, usually on timescales between $10^{-8} - 10^{-3}s$. The absence of heavy atoms makes this possibility even less likely. From the transient absorption data the researchers were also able to determine the triplet yield, which approached 200%. The data is displayed in figure 1.8B and 1.8D.

In conclusion, the study shows that N, N-bis(phenylethyl)-PDI performs singlet fission, and the triplets are produced faster than 200 femtoseconds, which was the time resolution of their setup. The timescales are consistent with the dynamic simulations using Redfield theory. Additionally, the yield of triplets approaches 200% in both amorphous and crystalline thin films. This work shows that this PDI derivative performs singlet fission. However, proving that it performs singlet fission does not necessarily mean that it will do so in a practical PV device, and this leads to the main objective in this thesis: "Proving singlet fission as the source of the generated photocurrent by the electron acceptor N, N-bis(phenylethyl)-PDI." PV devices with singlet fission materials as donor material exists already, albeit not with this PDI. The additional benefit of this PDI is the stability of the molecule and its electron accepting properties. In contrast with regular singlet fission devices the work described in this thesis will

aim to fabricate the first singlet fission solar cell with a molecular donor and PDI singlet fission acceptor.

1.6 PDI as an acceptor with PTB7 donor molecule

The goal of the research project was to successfully fabricate an organic solar cell with perylene bis(phenethylimide) as an acceptor that also performs efficient singlet fission. As such it is important to be familiar with the work that has been done on the PDI derivatives as acceptors in organic solar cells. Unfortunately, the perylene bis(phenethylimide) is a novel material that is currently not commercially available, and literature on this specific molecule as an acceptor is not available. Our donor PTB7 molecule has been combined with other PDI derivatives and these devices have shown great potential, reaching high power converting efficiencies for non fullerene based organic solar cells. We will discuss recent work on these devices and this will serve as a guide for our own experimental work. In a recent article by Zhong et al., a BHJ solar cell was fabricated from PTB7 and a PDI derivative.[86] The molecular structure of the PDI they used is shown in the figure next to the IV curve. It is produced by the fusion of two PDI units by a two carbon bridge. The LUMO levels are around the -4 eV and the moleucele shows relatively high electron mobilities and the highest absorption peak for this molecule is around 400nm.[85] The mass ratio of the PDI and the PTB7 was optimized,and they found that 7:3 PDI to PTB7 produced the highest efficiencies of 3.5% and 4.5%, for the non inverted and inverted structures respectively.[86] To enhance the devices further multiple solvent additives for improved mixing were investigated. 1-Chloronaphthlaene (CN) and diiodooctane (DIO) both significantly improved the performance of the devices, when added to the mix as $1\%_{vol}$. As can be seen in figure 1.11, the addition of the solvents mainly enhanced performance through increasing the fill factor, which went from 53.1% without additives to 55.6% and 54.5% with DIO and CN, respectively. When the two solvents were added together, the fill factor increased to 60%, and this led to the highest efficiency of the PTB7:PDI cell of 5.21%.[86] The IV-curves are displayed in figure 1.11 Although the obvious difference with our PDI, the results of this

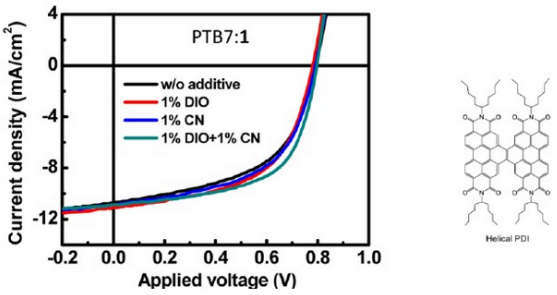

Figure 1.11: The IV curves with different solvent additives, and the molecular structure of the PDI molecule

cell motivated our attempt to use the PTB7 donor molecule with out PDI as an acceptor.

Chapter 2

Results and discussion

We will now focus on the experimental work performed throughout the internship, and discuss the results that were obtained. The perylene bis(phenethylimide) was, as stated previously, provided by a group at Delft University. The theoretical and experimental results from their research on this PDI molecule were discussed previously, and suggest that this molecule should perform singlet fission. The energies of the S_1 and T_1 states were calculated using time dependent DFT. The energetic requirement for singlet fission appears to be met, and the CT state was estimated using more detailed calculations that incorporate polarization of the the environment. For a more complete explanation regarding the theoretical calculations the reader is referred to [25]. The energies of the states were determined as following;

1. $E(S_0S_1) = 2.03eV$
2. $E(CT) = 3.1eV$
3. $E(T_1T_1) = 1.72eV$

2.0.1 Energy levels in the PDI material

UPS

As these are merely theoretical calculations, we thermally evaporated the PDI material onto Si:Au substrates and sent these samples to Cambrdige University for UPS measurements. In this experiment we measure the kinetic energy of emitted electrons which have absorbed high energy, typically ultraviolet, photons. This allows one to determine the HOMO energy level. The measurement is done in ultra-high vacuum. Determining the optical HOMO/LUMO gap is not so straightforward. The definition of the band edge is arbitrary, as it depends on a density of states. There are several ways found in literature, the most common approach is to linearly extrapolate the highest valence band feature of the UPS spectrum and define the band edge as its intersection with background level. Lastly, depending on the wavelengths used, surface effects can become pronounced in the data.

The measurements were performed at the Cavendish Laboratory, optoelectronics group at Cambridge University. The results are summarized in figure 2.1. The results provided valuable information on the HOMO level in our PDI molecule. With UV-VIS we can determine the bandgap, and adding this value to the HOMO level gives an approximation of the LUMO level. These energy levels are important for choosing materials to combine PDI with. As the triplet state is a dark state, the energy of the triplet state is not determined. As we can see from the UPS data, the PDI material has relatively deep HOMO levels. The HOMO is positioned at

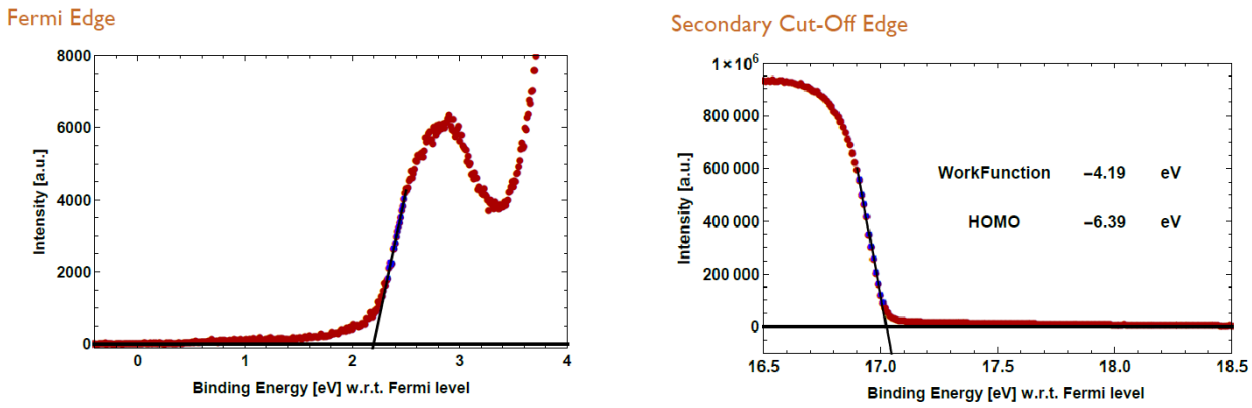

Figure 2.1: UPS data measured by Marcus Böhm at Cambridge University

approximately -6.39 eV, and this suggests that the material could be suitable as an electron acceptor.

For singlet fission the triplet level must be positioned close to half the energy of the S_1 level. This suggests that this PDI is an interesting molecule for singlet fission research, as the triplet level would then be closely positioned to the silicon bandgap value of 1.11 eV. If the PDI can efficiently absorb photons, produce triplets with an energy of around 1 eV and transfer these electrons to the silicon, it can be an interesting route to surpassing the Shockley-Queisser limit.

UV-VIS

The next step was to determine the absorption spectrum of the PDI, as this provides us with a way to estimate the bandgap of our material. The details of this measurements are described in the appendix, and the results are displayed in the left side figure 2.2. The absorption spectra

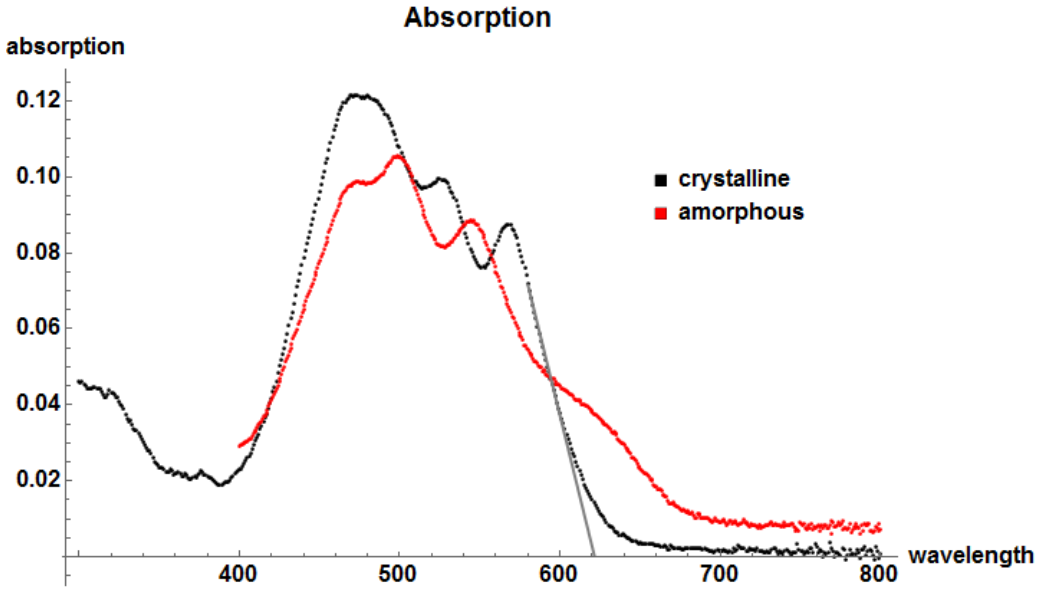

Figure 2.2: Absorption spectrum of PDI

provide a basic estimation of the bandgap of materials, and will also be useful when taking the external quantum efficiency of the films. The optical bandgap of the material can be found be

fitting a straight line from the onset of absorption. For crystalline PDI this is at 621.6 nm, implying an optical bandgap of ± 1.98 eV.

The group at Delft University performed transient absorption and time-resolved PL on both amorphous and crystalline films of the PDI, and applied substrate heating of the samples during deposition of 180°C to produce crystalline films. The PDI films for devices have layers underneath, some of which will deform/degrade at these temperatures. During the fabrication of crystalline layers we therefore opted to apply 130°C during PDI deposition. The deposition of the amorphous PDI layers was performed without any substrate heating. AFM measurements were performed to analyze the morphology of the PDI films.

2.0.2 Film morphology

The group at Delft University that provided the PDI have also taken AFM images. Although for the BHJ the morphology is more important than for the bilayer devices, for the bilayer this can also be informative. In organic solar cells the exciton has to reach an interface within 10 to 20 nm, failure will lead to recombination. In figure 2.3, the PDI film on quarts is displayed. The image of the PDI layer is a sample on quarts with heating of substrate holder during

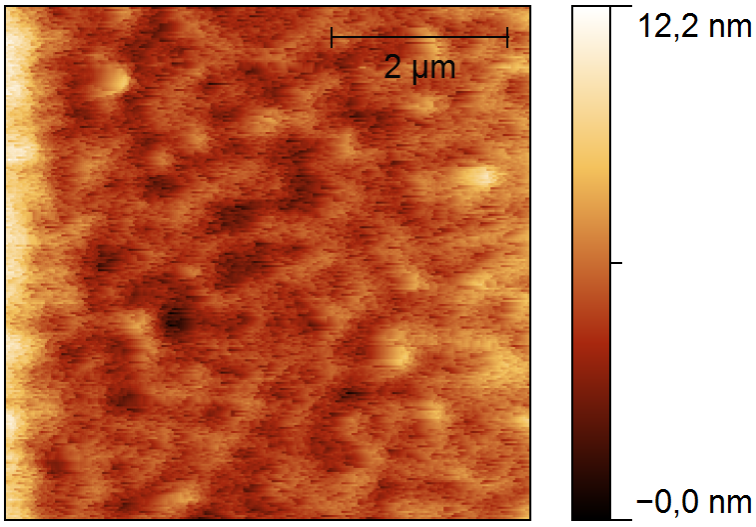

Figure 2.3: AFM image of the PDI film

deposition of 130°C and a deposition rate of 1 $\mathring{A}$ per second. The images of the bilayer cells provide information about the evaporated crystalline PDI layer. No AFM images were taken for the amorphous PDI films. As will be discussed in the device results section, the devices with an amorphous PDI performed significantly worse than the devices with a crystalline PDI layer.

The AFM images shows a smooth film of the PDI, and shows that the evaporation rate of 1 $\mathring{A}$ per second with 120 °C are appropriate evaporation conditions. Since this was a new material, the evaporator was not calibrated to yield the appropriate thickness of the PDI layer. Therefore we explored the film thickness using the Focused Ion Beam (FIB).

2.0.3 Film thickness

Aside from the morphology of the PDI layer, the thickness is also important for device performance. An active layer too thin will not absorb sufficient light to produce reasonable currents,

but when the active layer is too thick, the chances of the charges reaching the proper electrodes drop due to recombination and trap states. Two experiments were performed to explore the thickness of the layers in the devices, FIB for the devices and the profilometer to measure the PEDOT:PSS thickness. The profilometer confirmed the desired thickness of the PEDOT:PSS layer, for more information see appendix.

The Focused Ion Beam (FIB) is an instrument that is often a complementary technique to a Scanning Electron Microscope. In the FIB setup, a focused beam of ions, in our case gallium ions, is used to sputter a small amount of material off the surface, and cut away parts of the sample. Combined with a scanning electron microscope the electron and ion beams intersect at a point near the surface, which allows for high vertical resolution. For solar cells this is one of the only ways to acquire information about the vertical morphology of the sample. In figure 2.4, FIB images and the device structure are displayed.

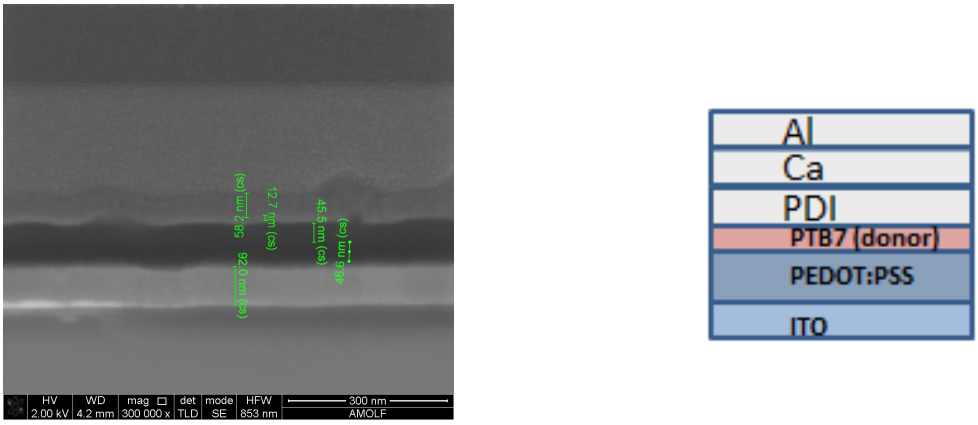

Figure 2.4: Left: the FIB image of the device. Right: Schematic outline of device

In the image we measured the thickness between the layers. It becomes clear from the images that the contrast between the spincoated PTB7 layer and the evaporated PDI layer is minimal. Therefore we cannot say anything regarding the thickness of this layers individually. We are able to distinguish the organic layers from the glass, ITO and the metal electrode. The thickness of the active layer is approximately 100nm, which is an appropriate thickness of the active layers in OPV cells.

2.1 The biliayer solar cells

The focus of the next part of the thesis are the fabricated devices. From the UPS measurements and from existing literature we know that PDI is a suitable electron donor.[86] We wanted to investigate the PDI in 2 different ways, using it as an electron donor and as an electron acceptor. For the devices with the PDI as an electron donor we adapted the structure from Congreve et al..[16] In the devices with PDI as an electron acceptor we adapted the structure from Zhong et al..[86] The cell structures are displayed in figure 2.5. None of the existing singlet fission molecules shows this property, and this could present a way towards an all-singlet fission solar cell.

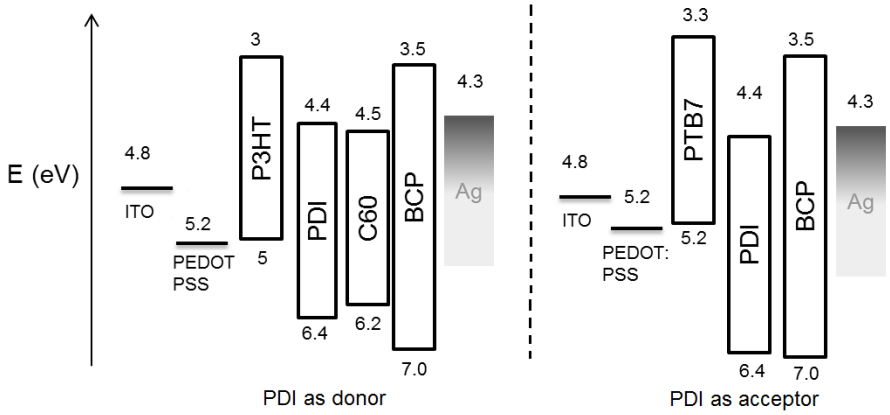

Figure 2.5: Left: cell structure with PDI donor. Right: cell structure with PDI acceptor.

2.1.1 Device performance of the bilayer devices

Device performance with PDI donor

Every batch consists of 16 solar cells, only the best performing cells are presented here. The IV-curves of the bilayer devices with PDI as an electron donor are shown in figure 2.6. On the left the IV-curve of a cell with 130°C heating applied during deposition, on the right an IV-curve of an amorphous sample is depicted. As becomes clear from the IV-curves, applying

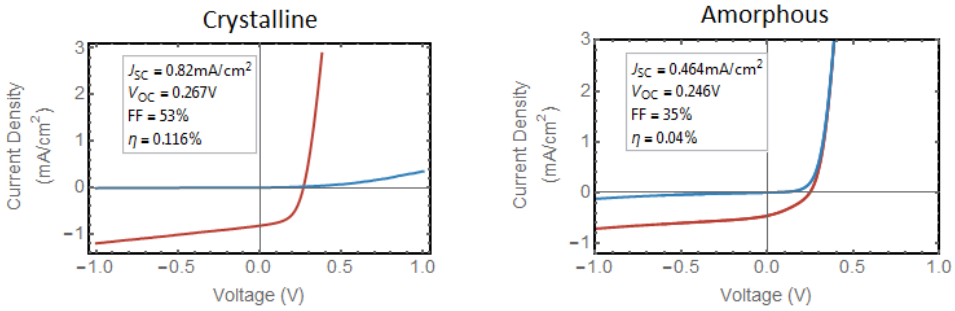

Figure 2.6: IV-curves of the crystalline PDI solar cell (left) and the amorphous PDI solar cell (right). Blue: dark IV. Red: Light IV

heat during the deposition of the PDI layer increases the device performance. From this point on we decided to consistently heat the substrates to 130°C during PDI deposition.

The IV-curves show a relatively low V_{oc}, which is probably the result of high recombination in the devices. From UPS and UV-VIS we know that the energy of the HOMO and the LUMO in the PDI are approximately -6.4 eV and -4.4 eV, respectively. For C60 these values are -6.6 eV for the HOMO and -4.5 eV for the LUMO. The difference in LUMO levels of the donor and the acceptor presents the driving force that separates the exciton at the interface. In this solar cell the difference is very small, and this small difference in energy between the LUMOs of these materials could have resulted in inefficient charge separation. This recombination would have a profound negative effect on the V_{oc}.

The interface area for bilayers is limited, which normally yields relatively low currents. The J_{sc} is doubled for devices with heating applied during PDI deposition, which is probably due to better charge transport properties of the crystalline film. The fill factor of 53% for the crystalline devices, and 35% for the amorphous, imply solar cells of good quality, with low series resistance and high shunt resistance.

Device performance with PDI acceptor

As mentioned previously, the unfavorable energy alignment of the PDI and the C60 resulted in a low V_{oc}, and the PDI should be more suitable as an electron donor. In figure 2.7 we see an IV-curve of a cell with a crystalline PDI layer, in combination with a PTB7 layer with a concentration of 10mg/mL with spun for 60 seconds at 2000RPM, which was our standard recipe. The bilayer devices of the PDI electron acceptor and the PTB7 donor material yielded

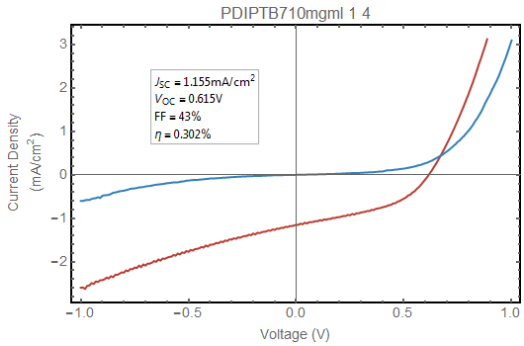

Figure 2.7: IV-curve of the first batch with PTB7 donor material

better results compared to the devices with PDI as electron donor. The J_{sc} of the cell is $1.155 mA/cm^2$, the V_{oc} is 0.615V and a fill factor of 43%. The maximum voltage that can come from an organic solar cell is equal to the difference of the donor HOMO and the electron LUMO. In practical organic solar cells we have to subtract 0.3V as a rule of thumb, due to the need for energy offsets to drive the charge carriers to their respective electrodes. In our device this difference between the donor HOMO and the acceptor LUMO is approximately 0.8V, and the V_{oc} of 0.6V is a nice achievement. The offset in LUMOs between the PTB7 and the PDI is significantly larger in these devices, and this has probably resulted in more efficient charge separation at the donor/acceptor interface. The J_{sc} is also enhanced for these cells, although it remains relatively low. The bilayer device architecture suffers from a low interface area, and thus always performs significantly worse than their BHJ counterparts.

Overall, the performance of the solar cells with PTB7 donor material was promising. The diode behavior in the dark curve is not optimal; the dark curves shows pseudo-linear dependence on the applied forward bias, instead of an exponential dependence. This means that when the charge passes through the diode, it experiences resistance in the path towards the SMU, in our devices the active layers and the extraction layers (in our device the PEDOT:PSS). However, optimization of this device structure did not yield better results.

2.1.2 EQE

Exploring the photocurrent response of the PTB7/PDI bilayer device for different wavelengths allows us to assess the origin of the photocurrent. If we see photocurrent following illumination with photons with an energy in the region of the PDI absorption, this shows that PDI produces photocurrent and would allow us to probe the effect of an external magnetic field to detect possible singlet fission. If the amount of current is much higher in the absorption region of the different components, here the PTB7, then it will be difficult to observe a change of a couple of percent in photocurrent due to an external magnetic field, which is the change one expects in singlet fission magnetic field studies. The EQE measurements were performed on the bilayer samples with the PTB7 layers produced as follows: 5mg/mL spun for 60 seconds at 2000RPM, and annealed at 100°C for 20 minutes. This concentration is half the concentration of our

standard recipe. The results are displayed in figure 2.8. From the data above we see that the

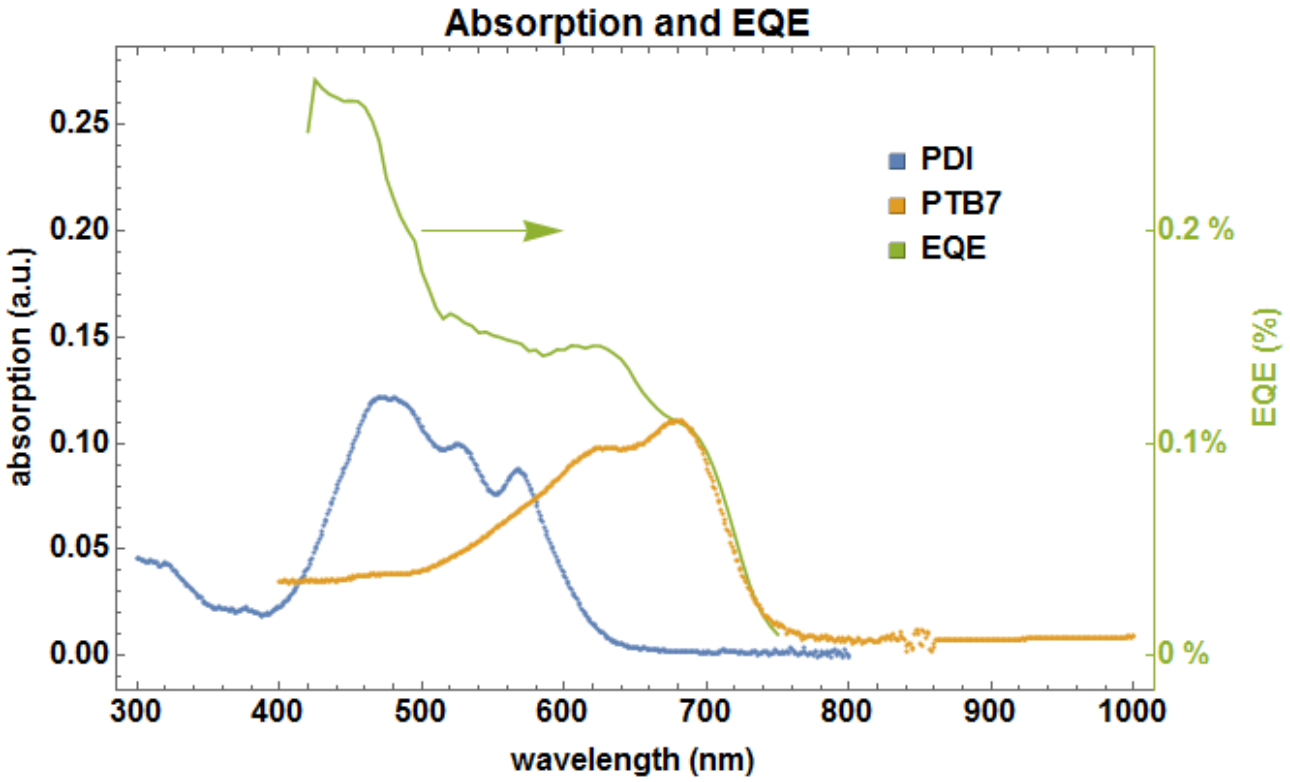

Figure 2.8: Results of the EQE measurements and the absorption spectrum of the PDI and the PTB7

EQE values are very low, below 1%. The EQE measurements were taken with an EQE setup that operates at high power (1000 suns), and can only be used with the sample exposed to air. For the PDI should be stable in air, however, PTB7 is unstable in air. The high power of the EQE setup could be another reason for the low values obtained. High power light is likely to induce light-induced degradation and increased recombination. All in all this could have resulted in the EQE results not being compatible with the currents measured on the devices. Integration of the EQE over the solar spectrum should yield the J_{sc} of the solar cell under the solar simulator. The EQE obtained is too low to comply the J_{sc} of the devices.

However, this was not the reason why we were interested in the EQE. If the EQE curve shows features at the absorption peaks of the PDI, it means that the PDI produces photocurrent, as can be seen in figure 2.8. The main absorption features of PDI can be mapped onto the EQE spectrum. From this result we concluded that, although there is very little current produced by the cell, a part of it comes from the PDI. This encouraged us to continue the research on this type of cell, and in particular to probe the effect of a external magnetic field on the photocurrent.

The results from the IV measurements, together with the EQE results that show that both the PTB7 and the PDI produce photocurrent, encouraged us to explore the singlet fission properties of the PDI. In order to detect singlet fission, the photocurrent response to a magnetic field has to be probed. To take reliable measurements the photocurrent should be as high as possible, as this will yield the best signal-to-noise ratios. The change in photocurrent observed in singlet fission cells is 1-5%. To increase the photocurrent, and overall efficiency, we decided to fabricate BHJ solar cells, which have higher interface areas and typically result in the best performing organic solar cells.

2.2 Bulk heterojunction solar cells

From literature we know that PDI derivatives dissolve best in halogenated organic solvents, and produce best results with diiodooctane as a mixing solvent. We opted for a solution of chlorobenzene with 30mg/mL concentration, and a small amount of diiodooctane ($1\%_{vol}$). In total we made 3 batches of BHJ solar cells. The solar cells had the following structure.

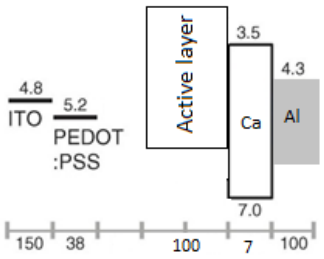

Figure 2.9: Schematic outline of BHJ device architecture

In BHJ solar cells the mixing and resulting morphology are crucial for cell performance. We varied the PTB7/PDI ratio between [1 : 1.8], [1 : 2] and [1 : 2.2], because the weight ratio varies in literature between [1:1] and [3:7]. Common solvent additive concentrations are between $0.5 - 3\%_{vol}$ in literature.

When filtering the prepared solutions for the first batch prior to the spinning, we noticed that the liquid did not pass easily through the filter. With the application of force the liquid turned foamy and passed through. Solar cell performance was poor, and visible aggregation could be seen on the samples by eye. The molecules did not dissolve properly, probably because the solutions were not stirred and heated sufficiently, and this resulted in the substandard device performance. For the next batches we applied 80°C to the solution with active layer ingredients, and stirred for several hours.

2.2.1 BHJ device performance

Instead of enhanced cell performance we experienced the opposite. The currents hardly exceeded $0.03mA/cm^2$. In figure 2.10a, the IV-curve of one of the BHJ cells is shown. This IV-curve is from the batch without problems encountered during the filtering of the solution. THis sample was a made with a [1 : 2] PTB7:PDI ratio, $1\%_{vol}$ DIO and 20 minutes at 80°C annealing after the spincoating of the active layer.

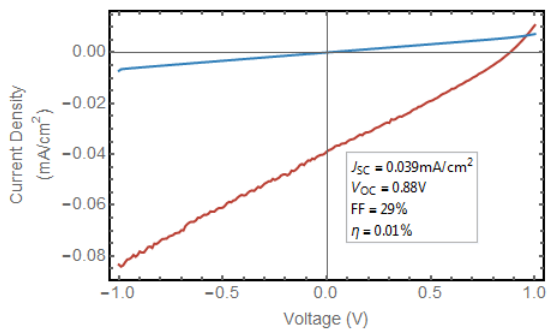

Figure 2.10.a: IV-curve of BHJ cell

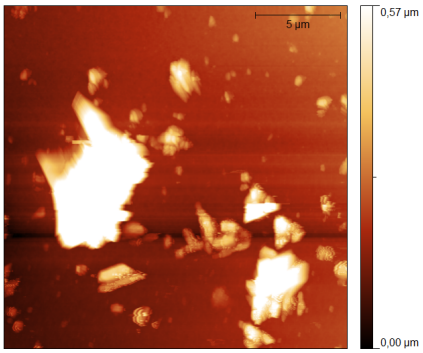

Figure 2.10.b: AFM image of BHJ solar cell

The BHJ devices produced less current than the bilayer cells. This is probably due to the inmiscibility of PTB7/PDI combination. Another possibility is that the solvent did not dissolve on of the ingredients, which would have negative effects on constitution of the active layer in our devices. Although the voltage has increased, which normally happens in solar cell with very low currents, the overall performance was substandard. As the morphology of BHJ solar cells is crucially important for device performance, and there are several parameters that should be optimized, we cannot conclusively say that these materials together simply do not work. We have taken an image with the AFM. The AFM image was taken for the same sample as the IV-curve in figure 2.10b. The AFM image shows large features on the film (which were present on the whole film), and we assume these are PDI aggregates, as PDIs have a tendency to aggregate in films. This morphology will not result in high performing solar cells. After the 3 unsuccessful attempts we concluded that we did not have sufficient time for several rounds of optimization, and thus continued the research with bilayer cells. At this point we have OPV devices with a PDI electron acceptor which, presumably, performs singlet fission. From the EQE measurement we know that the PDI produces current in our devices, which allows for the investigation of singlet fission through probing the effect of an external magnetic field on photocurrent.

2.3 Magnetic field dependency measurements

The magnetic field dependence of photocurrent of our solar cells could confirm if singlet fission is taking place in our solar cells. However, the currents from our solar cells were low at 1 sun, and the LED used to specifically excite the PDI (490nm LED) was weak, which resulted in the fact that the measurements were in the sub-nanoampere region of which only a part is current from the PDI. We tried the setup on several cells, both BHJ and bilayer cells. To detect singlet fission in a solar cell the photocurrent should decrease with the strength of the magnetic field, with a stabilization after 3000-4000 Gauss. The decrease one expects in these experiments is in the order of 1%-3%. For our solar cells this means we expect a decrease of 2% of ± 3 nanoamperes, i.e. 6×10^{-11} amperes. This makes the change hard to measure, as things such as air flows, and movement of the cables, can induce currents of these magnitudes. Figure 2.11a shows that there is too much variance in the measurements to be able to detect a trend. The computed RMS for the measurement was 25%. In figure 2.11b the expected change for both the photocurrent and the PL is shown, and the data was obtained from Wu et al..[83]

Individually each measurement an average over 100 integrations of 5 seconds. Similar results were obtained during multiple other attempts of probing the photocurrent response to an external magnetic field. With the variation in our measurement we are unable to detect the change we expect.

2.3.1 Not enough current?

The low currents in our devices might present a problem in our experiments; the signal change is very low compared to variation in the measurement. Therefore we performed an error analysis. The measurement includes a lot of sources of error while the relative change in photocurrent we expect is small. We have estimated whether the setup is capable of measuring these changes. The possible sources of error we have identified are:

1. Uncertainty in the Lock-in Amplifier
2. The position of sample in the sample holder, and connection to the wiring

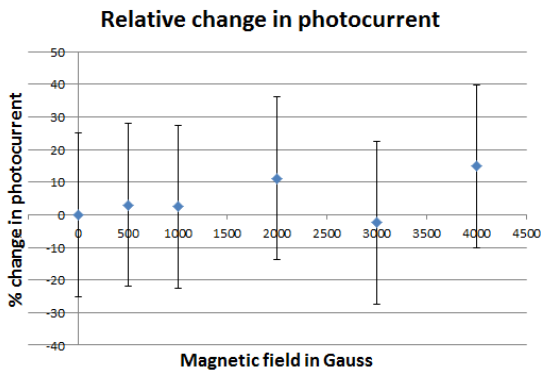

Figure 2.11.a: Photocurrent as function of magnetic field

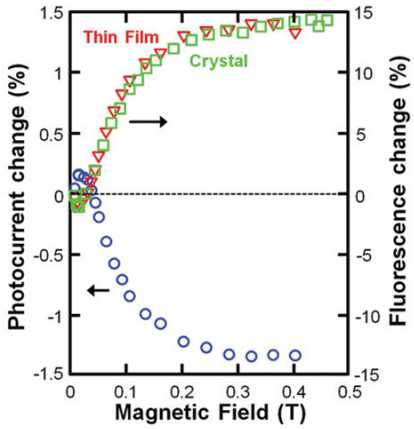

Figure 2.11.b: Dependence of photocurrent and PL on magnetic field strength in pentacene. Source: Wu et al.[83]

3. Uncertainty in the strength of the magnetic field
4. The drift current during the measurement
5. Position of the sample holder in the magnetic field

After taking several measurements for the sources of error, we concluded that the most significant source of error is the position of the sample in the sample holder, and the connection between the sample holder and the wires. The variation in photocurrent due to changing this parameter were very large, 50-60% were not uncommon. The standard deviation turned out to be 1.155 nanoampere. The average value of the photocurrent measurements was approximately 4 nanoampere, meaning that the relative standard deviation is 25%. The change in photocurrent expected is definitely below 10%, and therefore we can conclude that, using our setup, we are not able to measure the change in photocurrent due to large deviations resulting from altered connection of the sample(holder).

We need a more accurate experiment to detect singlet fission in our samples. Therefore we performed PL studies on pure films of PDI material. As is shown in figure 2.12b, the expected change in photocurrent is larger than the expected change in photocurrent.

2.4 PL in magnetic field

After the unsuccessful attemps to detect a change in photocurrent due to an external magnetic field, we probed the PL response under an external magnetic field field. Whereas the effect of a magnetic field on the photocurrent of a device depends on subsequent processes such as charge separation, charge transport and extraction, measuring the PL presents an easier way because the singlet exciton only has to radiatively decay for a signal to be detected, and the expected change is larger. Additionally, the high variation of the photocurrent measurements due to the connection to the sample holder is another problem that is circumvented in the PL measurements. PL from the PDI films should be almost completely fluorescence, as no heavy atoms are present that can facilitate spin-orbit coupling. Singlet fission rates are reduced when an external magnetic field is applied, and this means that if the PDI performs singlet fission, the observed PL should increase when the magnetic field is turned on because the S_1 radiatively decays back with less competition of singlet fission. We used a 405nm laser, used a 425nm filter

to prevent signal directly from the laser, and took 5 measurements with an integration time of 2 seconds for every condition. From the group at Delft University we know the emission spectrum of the PDI, which is displayed in figure 2.12. The films measured in figure 2.13 were deposited

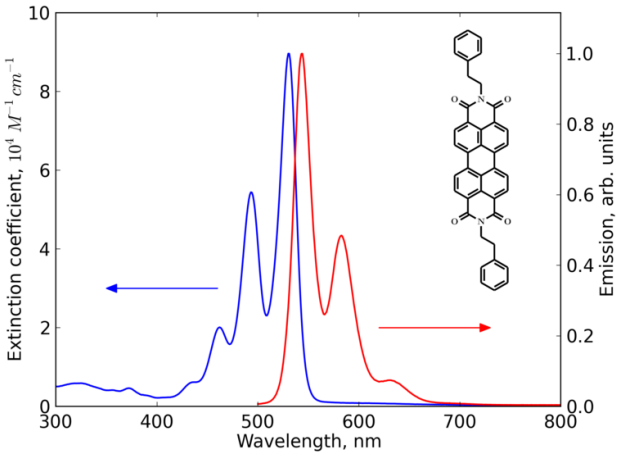

Figure 2.12: Absorption and emission spectrum PDI

6 months prior to the PL-measurement, from a different batch of PDI. The evaporation details were $1\mathring{A}$ per second rate, substrate heating to 120 °C during the deposition and a thickness of 35nm. In all the difference-curves we subtract the signal without the magnetic field from the signal from the magnet-on condition. Positive signals in these curves thus suggests singlet fission due to an increase in PL created by the magnetic field. We see a clear emission feature

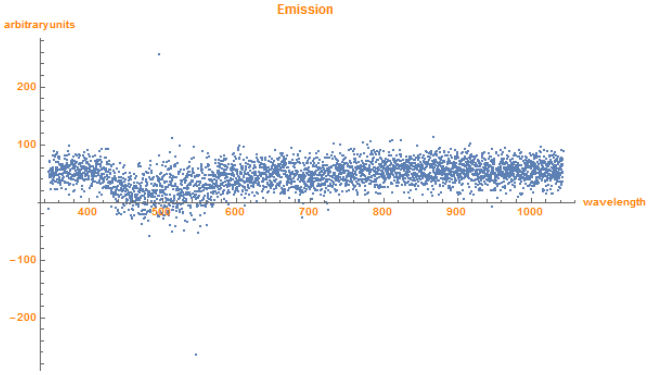

Figure 2.13.a: PL difference

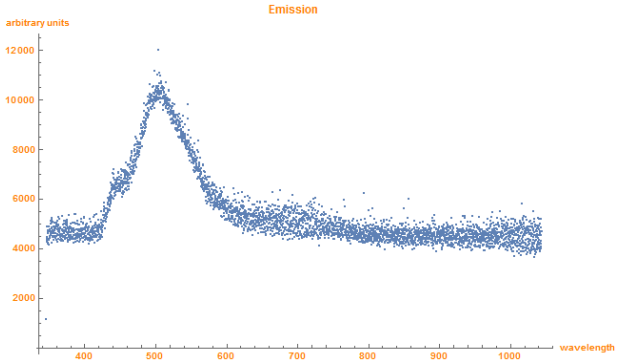

Figure 2.13.b: PL without magnetic field

with a peak around 510 nm. This does not comply with the UV-VIS experiments, which can be seen in figure 2.2. The emission should be red-shifted from relative to the emission, and the emission peak almost coincides with the absorption peak. The emission is compatible with the data from Aulin.[2] However, there is no increase in PL when the film is placed in a magnetic field, suggesting that there is no singlet fission.

The second type of films measured were deposited on quarts glass at a rate of $3\mathring{A}$ per second without any heating of the substrate holder during the deposition, and had a thickness of 50nm. Whereas for the old film we observed a green emission, a sharp red emission was observed for the new samples. This can also be seen in figure 2.14. We now see a clear emission feature at approximately 700 nm. From the measured UV-VIS spectra in figure 2.2, this is where we expect the emission to be. The PL does not significantly increase in the presence of a magnetic field. We measured the background signal for the measurements to investigate

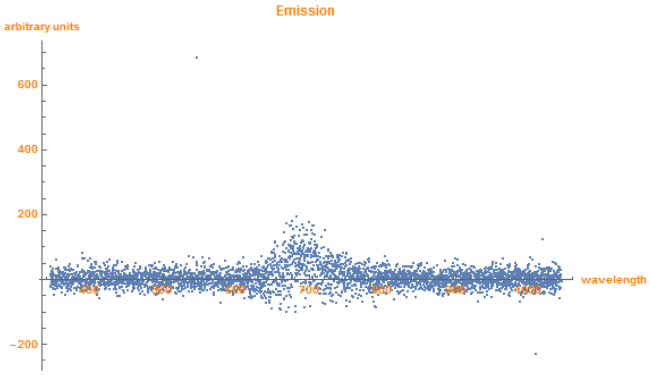

Figure 2.14.a: Difference in PL; Signal magnet on - signal magnet off

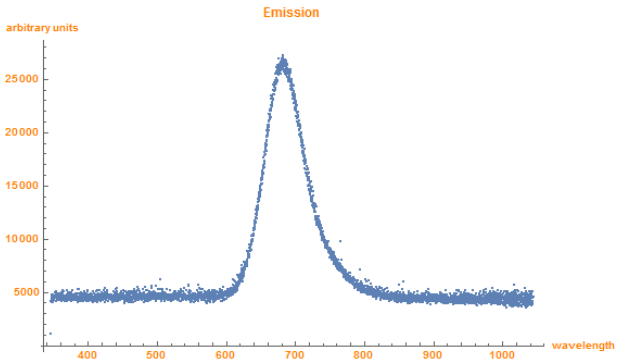

Figure 2.14.b: PL without magnetic field

whether this could be causing the difference in emission features, as displayed in figure 2.15. This does not show any features in the wavelength regions of both the emission from the old film or the new film. The PL in the wavelength region of the emission from the old films has

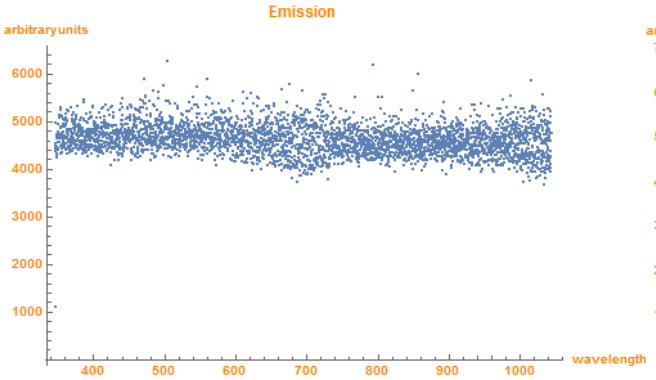

Figure 2.15.a: Background with the magnet

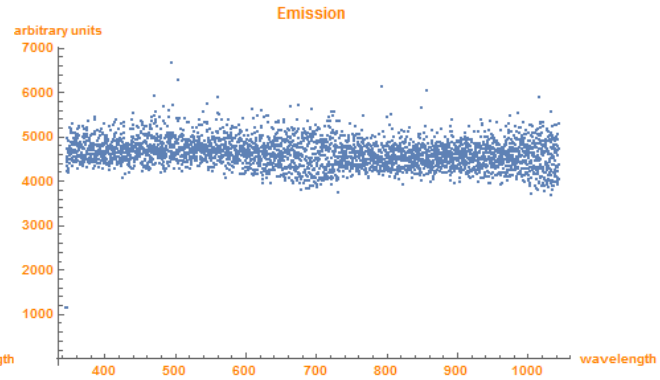

Figure 2.15.b: Background without magnet

completely disappeared. This suggests that the PDI films from this batch has a remarkably different emission spectrum than the PDI from the first batches of the project. We annealed the film at 140 ° C for 30 minutes to explore the effect of this annealing. This changed very little for both the absorption and emission spectrum. We therefore conclude that singlet fission is not significant in these samples. Every sample was measured 5 times in an "off/on/off/on/off" manner. The difference-graphs in the data is the average of the 2 "on"-signals minus the average of the 3 "off"-signals. Analysis of the individual runs, by computing the difference in consecutive measurements, yielded an interesting result in 1 case, and is displayed in figure 2.16.

The difference in PL we expect is a 5-15% increase, as these are typical values in singlet fission magnetic field dependent PL studies.[83] In figure 2.16b we see the total value of the PL signal without the magnet, which implies that the change we observe in this particular run is small.

Thus, we fabricated new films the same way as the old films were made. We heated the substrates during deposition to 120°C, and the rate was decreased from $3\mathring{A}$ per second to $1\mathring{A}$ per second. The data is displayed in figure 2.17. Again no change was observed between the magnet on and magnet off condition. We then annealed the film at 210 °C for 1 hour, to improve the crystallinity, but this yielded no change. As the new material showed a consistent emission feature with a completely different wavelength, we expect that the reason lies in the material

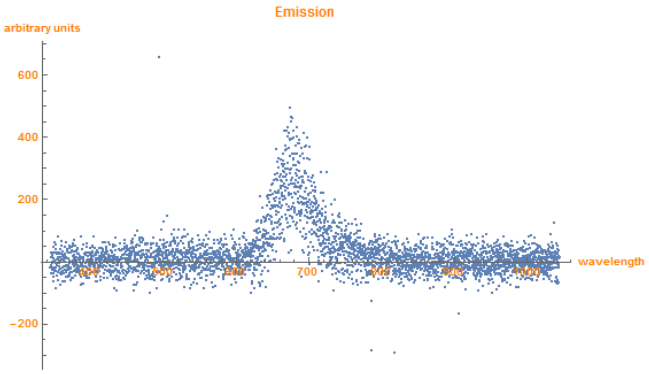

Figure 2.16.a: Difference in PL; Signal magnet on - signal magnet off

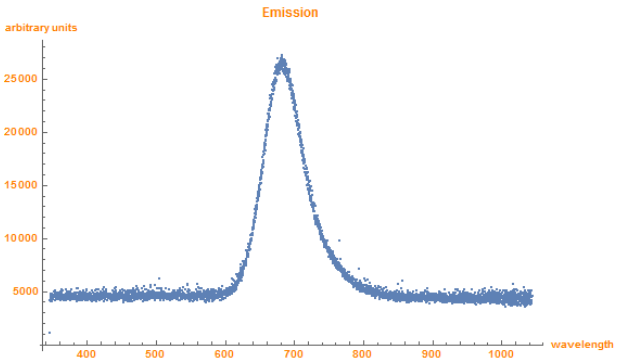

Figure 2.16.b: Signal without magnetic field

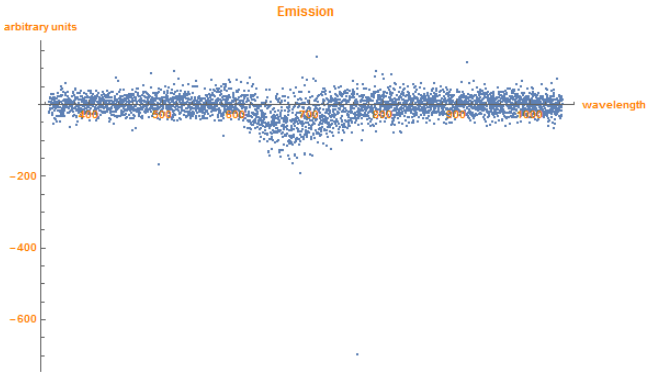

Figure 2.17.a: Difference in PL; Signal magnet on - signal magnet off

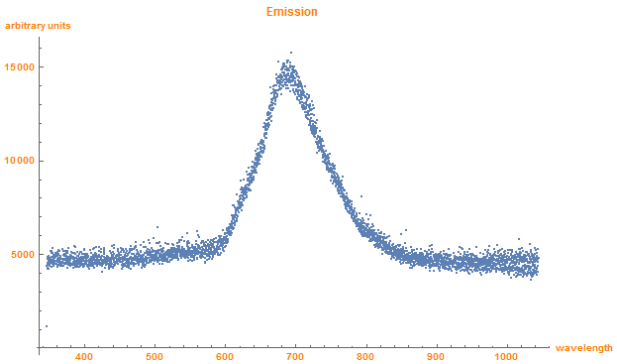

Figure 2.17.b: PL without magnetic field

itself. The absorption spectrum is almost unchanged compared to the absorption spectrum of the old films, merely the emission. The origin of this effect is unclear, but is likely due to the degradation of the films over time due to water, air or light.

From the PL measurements we conclude that there is no significant singlet fission in our thin films.

Chapter 3

Conclusion

Researchers at Delft University investigated the singlet fission properties from perylene bis(phenethylimide). Transient absorption studies show an ultra-fast (within 150 fs) stimulated absorption peak, and the energy of this transition corresponds with literature on triplet absorption features in PDIs.[19] Because there are no heavy atoms present in the PDI, they assume this triplet population can only be the result of singlet fission. Time-resolved PL experiments also showed a significant decrease in the S_1 lifetime in thin films compared to the S_1 lifetime in solution. Together with the theoretical energy calculations that confirm the slight exoergicity of singlet fission in this system, this suggests that this molecule could perform singlet fission in practical OPV devices. Through literature and UPS and UV-VIS experiments, we know that the PDI should be a suitable energy acceptor. No singlet fission molecule exists that shares this suitability as electron acceptor, and successful integration of a singlet fission donor and acceptor could yield the first all-singlet-fission solar cell and theoretically prevent even more thermalization losses. We fabricated devices both with PDI as a donor and as an acceptor, combining it with a C60 acceptor and the PTB7 donor, respectively. The performance of the devices with PDI as a donor were relatively substandard, and this was as expected due to the deep energy levels of the PDI and the resulting high levels of recombination. The results with PDI as an acceptor and the PTB7 donor molecule were better. The higher V_{oc} implies lower recombination rates and the J_{sc} of 1.115 mA/cm^2 is not bad for bilayer device. Switching to the BHJ architecture did not yield satisfactory results, as the J_{sc} was now decreased to approximately $0.04 mA/cm^2$ on average, and as a result the V_{oc} increased. AFM measurements of the BHJ surface show large features, hundreds of nanometers in size, that indicate large scale separation of the donor and the acceptor. Another problem that could have caused the unsatisfactory results is the incomplete dissolution of 1 of the active ingredients. EQE studies on the bilayer devices with PDI acceptor showed that, although EQE is low due to high powers and the measurement being done in air, some of the current originates from the PDI. Subsequent measurements of the dependence of photocurrent on an external magnetic field were unsuccessful. The main issue during the measurements was the low performance of the solar cell, which, in combination with the use of a low-power LED, resulted in very low currents. The expected 1-3% change in photocurrent requires the accurate detection of changes of 20-30 picoamperes. The measurement was severely impeded due to the loose connection of the sample holder and the wires, which resulted in a RMS of 25% of photocurrent. This means that even if we observed a change in photocurrent of 2%, this would all fall well in the standard error.

A more accurate way to detect singlet fission is to probe the PL dependence on an external magnetic field. By suppressing singlet fission with the magnetic field, we should detect stronger PL. The expected change is larger, because it does not depend on charge transport and extrac-

tion like photocurrent. The expected change is now 5-15%, and with the RMS of 0.7% in our measurement, detection should be possible. However, no increase in PL was observe when the magnetic field was present, suggesting little or now singlet fission occurring in our thin films of PDI.

In the end we must conclude that the perylene bis(phenethylimide) could not live up to the expectations from the transient absorption measurements from Delft University, as we did not detect any singlet fission. The researchers at Delft University base their suspicion of singlet fission in this material predominantly on the TA measurements and the time-resolved PL measurements. The appearance of an absorption feature in the TA within 150fs, at an energy that corresponds to triplet-absorption in literature, is not conclusive evidence for singlet fission. The high intensity of the TA measurement might induce various processes that are not realistic under 1 sun illumination. Additionally, the possibility of this feature being an absorption of the S_1 state to a higher singlet excited state cannot be ruled out, as limited work has been done on perylene bis(phenethylimide). Ideally the transient absorption features with and without the presence of an external magnetic field should be compared, which could provide a stronger indication of singlet fission (or its absence).

The time-resolved PL studies that indicated a significant shortening of the S_1 lifetime in thin film compared to its lifetime in solution, also does not provide conclusive evidence for singlet fission. It is not impossible for the S_1 lifetime to be significantly shortened by the presence of neighboring molecules. The decay kinetics must be explored further, and evidence for the presence of both prompt and delayed fluorescence should be found, together with the alterations due to an external magnetic field.

We have not detected significant singlet fission in perylene bis(phenethylimide). Having electron acceptor properties, singlet fission detection in this molecule would present the first singlet fission electron acceptor. This could be a worthwhile endeavor because all-singlet-fission solar cells could provide an even better coverage of the solar spectrum. It is therefore necessary that more work is done to determine whether this molecule can perform singlet fission in practical organic solar cells.

Chapter 4

Appendix

We will now present a brief explanation of the experimental details during both the fabrication and the multiple ways of characterization.

4.1 Methods of the characterization

4.1.1 IV curves

The source measure unit used was a Keithley 2401 SourceMeter Source Measure Unit (SMU) purchased from Tektronix. The solar simulator is an Oriel Sol2A. The lamp was warmed up before so that it produces 1 sun during the measurements.

4.1.2 UPS

For this measurement the PDI layer is thermally evaporated on a Si:Au substrate. These samples were then sent to Cambridge University where the samples were transferred to the ultrahigh vacuum chamber (ESCALAB 250Xi). The UPS measurements were performed using a double-differentially pumped He as discharge lamp emitting He I radiation of 21.22eV, with a pass energy of 2ev. The spectra are shown as a function of binding energy with respect to the vacuum level, and the energy edge of the valence band is used to determine the ionization potential of the measured film.

4.1.3 UV-VIS spectroscopy

The apparatus measures accurately between 300nm-1100nm, but going to such high energies is not practical in our case due to the onset of PEDOT:PSS and ITO absorption in these ranges. All these measurements were taken using a PerkinElmer 750 Lambda UV-VIS system, and both a 0% and 100% transmission were taken before a round of measurements.

4.1.4 Atomic Force Microscopy

The microscope that we have used during the experiments was purchased from Digital Instruments

4.1.5 Magnetic field measurements

The LED used during the magnetic field experiments was the LED490-02 (490nm), purchased from Roithner Lasertechnik. To obtain a higher signal to noise ratio, we used a Ametek Signal Recovery 7270DSP Lock-in Amplifier, and a Rigol DG1062 function generator. The magnet is a GMW 3470 elctromagnet, and the currents were measured using Keithley 2401 SMU. To prevent interference with the background light we opted for a frequency lock-in of 70Hz during all the measurements.

4.1.6 PL spectroscopy

The magnet used was the same as the one used in the photocurrent magnetic field studies. The monochromator was an Ocean Optics USB400, and we used a 425nm filter purchased at ThorLabs. We used a 405nm laser (Thorlabs) with a filter that does not allow passage for light with a wavelength below 425nm. This is to prevent a strong signal from the reflection of the laser. We decided to take 2 seconds as an integration time, and made 5 measurements. As we wanted to probe the effect of an external magnetic field accurately, 1 measurement of 10 seconds does not suffice. We started each measurement without the magnetic field, and after the measurement we turned on the output to the magnet which would then receive 5 ampères and create a magnetic field of 5000 Gauss at the position of the sample. We waited 10 seconds after turning on/off the output before we take the second measurement, allowing the field to stabilize. This we repeated until we had a total 5 measurements, which allows us to judge the effect of the field.

4.2 Methods during fabrication

The following procedures were not change during the measurements, and have been optimized in numerous other experimental studies. To this group belong the cleaning of the ITO and quartz substrates, the ozone surface treatment, the spincoating of PEDOT:PSS and the subsequent annealing processes and the spincoating of the P3HT. We will now describe these procedures.

4.2.1 Cleaning of the ITO and quartz substrates

ITO substrates are cut using a laser into substrates of 15mmx15mm, and upon unpacking are placed on a teflon platform with the ITO facing up. A beaker of the corresponding size is filled with deionized water and micro90 detergent (Sigma Aldrich) so that the substrates are totally immersed when placed in the beaker. After sonication for 20 minutes, the substrates are taken out and rinsed gently with deionized water. The substrates were then immersed similarly in acetone and sonicated for 20 minutes, and, after again rinsing with deionized water, the same protocol is performed with isopropanol. When all the cycles were completed, the samples were dried with a nitrogen blower and heated in an oven at 100 ° overnight. The procedure is similar for the quartz substrates. The quartz samples were purchased from University Wafers.

4.2.2 Ozone surface treatment

The dried samples are placed in the plasma cleaner, with the ITO patterning facing up. The chamber is closed and pumped down for 20 minutes to establish high quality vacuum. The gas valves were then opened with desirable power and plasma generation was turned on. After 30

minutes the generation was stopped and pumping down was continued for 5 minutes to prevent ozone release.

4.2.3 Spincoating of PEDOT:PSS

The PEDOT:PSS was stored sealed in the chemical cabinet, shielded largely from light and protected using parafilm. The PEDOT:PSS is filtered twice using 0.45μmeter PTFE filters after 30 minutes of sonication. A demo run is performed with the appropriate recipe to check whether the spin-coater was working properly. The settings for the spinning are as follows: 4000RPM for 60 seconds, and on every substrate 60 μL was applied.

4.2.4 Thermal annealing of PEDOT:PSS

After the spincoating of PEDOT:PSS, the samples are either annealed in the glove-box, or in the downflow-cabinet. The annealing temperature, on the other hand, was always kept at 120 °C, which is in accordance with existing literature. Another variation of annealing was that in the batch with the PTB7 donor molecule, certain samples were first annealed for 10 minutes in the downflow-cabinet and thereafter 20 minutes in the glove-box.

Profilometer

In the fabrication of the all devices we aimed for a PEDOT:PSS layer thickness of roughly 20nm. The profilometer uses a system which does not allow one to save the data, it merely serves as a quick check to determine the thickness of the spincoated layer. The picture from the screen was taken with a phone a phone, and this is shown in figure 2.4.

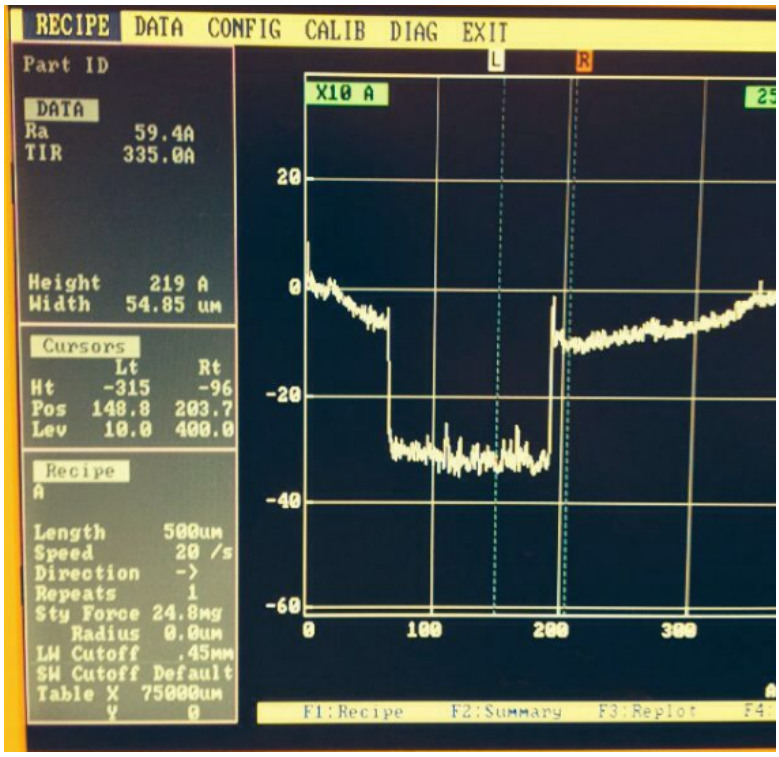

Figure 4.1: Thickness of the PEDOT:PSS layer determined with profilometer

4.2.5 Spincoating of P3HT

The P3HT that we used is stored in the glove-box, and was dissolved in chlorobenzene to a concentration of 4 mg/mL and then heated and stirred at 60 °C for 30 minutes. Once fully dissolved, the P3HT was filtered with a 0.2 μmeter PTFE filters and spun at 2000RPM for 60 seconds onto the PEDOT:PSS coated substrates. After this procedure, the substrates were subsequently baked at 110 °C for 20 minutes to remove any residual solvent. The substrates could then directly be transferred to glovebox where the evaporator is connected to, and were loaded appropriately into the sample holders.

4.2.6 C60 evaporation

The standard recipe was used for C60, and evaporation began at roughly 380 °C, and we aimed for a rate of 1 $\mathring{A}$ per second.

4.2.7 PDI handling and evaporation

The PDI was stored in the glove-box in a nitrogen atmosphere until used. In principle it should be relatively stable in air, but to prevent any degradation we stored the vials in the glove-box anyways. The crucible used for the thermal evaporation of PDI was previously used for tetracene. The crucible was emptied out as much as possible and then cleaned in the thermal evaporation chamber up to 900 °C, starting from 0 and thermal steps of 100 ° after which the temperature was kept constant for 20 minutes every time. The evaporation was started below 9×10^{-7} Torr, and starts around 260 °C varying somewhat with the quality of the vacuum. The rate we chose for PDI deposition was 1 $\mathring{A}$ per second in every solar cell batch, and it will be specified per batch whether or not the samples were heated during the deposition of the PDI. The evaporator was purchased from Angstom Engineering.

4.2.8 Spincoating and thermal annealing of PTB7

PTB7 is a polymer, and usually is dissolves best in halogenated organic solvents. We used 10 mg/mL concentration of PTB7 dissolved in chlorobenzene. PTB7 was purchased from Derthon Chemicals.The films are prepared using a spin-speed of 2000RPM for 60 seconds. Afterwards the films are thermally annealed at 80 °C for 10 minutes. As PTB7 is vulnerable to oxidation, the films are kept in the glove-box.

4.2.9 Thermal evaporation of metal electrodes

To facilitate proper sublimation the process is carried out at low pressures, approximately between $10^{-5} - 10^{-8}$ Torr. We started the deposition of organics only when pressures of 10^{-7} Torr were reached. Deposition of metals were sometimes started at 10^{-6} Torr. The rate we aimed for during the evaporation of metal layers was 1 $\mathring{A}$ per second, rates for other materials are stated when relevant.

4.3 Device fabrication

4.3.1 First batch with PDI donor

During this batch we combined the PDI as a donor with C60 as an acceptor, including PEDOT:PSS and P3HT layers between the PDI and the ITO. The thickness of the PDI layers was varied between 15-35 nm to explore the effects of different thicknesses. On top of the C60 acceptor layer a thin layer of BCP was deposited and the top electrode consisted of silver. The thinnest cell had a 15 nm PDI layer and the thickest 35nm. Significant PDI deposition started around T=260 °C, with 5×10^{-7} Torr vacuum quality.

4.3.2 Second batch with PDI donor

For the second batch did not change anything except for applying heat to the substrate holder during the deposition of PDI. The temperature applied was 130 °C, after consultation with the group at TU Delft that supplies us with the material. We only heat the substrates when the evaporator nearly achieved a stable deposition rate. The ramp rate of the substrate heater was set to near maximum values, 80 °/minute. This unfortunately led to an overshooting of the 130°C and maximum substrate temperature was 143 °C.

4.3.3 Batches with PDI as an acceptor with P3HT donor

We combined the PDI with P3HT as a donor. The spincoating of the P3HT was performed similarly to the P3HT layers used as an interlayer between PEDOT:PSS and the PDI in previous batches. The spincoating of PEDOT:PSS and the subsequent annealing also remained the same. We decided to continue with 30nm as the standard thickness of PDI. The thickness of the calcium layer was 5nm and the aluminium top electrode was 100nm thick.

4.3.4 Batches with PDI as an acceptor with PTB7 donor

For this batch we used PDI as an acceptor and P3HT as a donor. We substituted the P3HT donor with PTB7. The calcium layer was again 5nm thick and the aluminium top electrode 100 nm. We decided to go for 10mg/mL and 5mg/mL PTB7 solutions in chlorobenzene. The PTB7 was dissolved in chlorobenzene with a concentration of 10mg/mL, which was stored in the glovebox. In the glovebox the PTB7 was filtered using $0.45\mu m$ filters after it was heated slightly, at 60 °C, to improve quality. The spinning of the both PTB7 solutions was done at 2000rpm for 60 seconds. One group was annealed at 130 °C for 20minutes, another group of samples at 100 °C for 20 minutes and the last group was further processed without any annealing.

4.3.5 BHJ batches

For the BHJ cells we used for a solution of chlorobenzene with 30mg/mL concentration active ingredients, and diiodooctane as an mixing solvent. We chose to try the w/w ratios 1 : 1.8, 1 : 2 and 1 : 2.2, because the weight ratio of the donor and the acceptor varies in literature between [1:1] and [3:7]. A common solvent additive is diiodooctane (DIO), and the $\%_{vol}$ varies from 0.5% to 3% in literature. After the spinning of the active layer, which was done at 1500RPM for 60 seconds to create active layers of 100nm thickness, we anneal through 3 conditions, 1 without any annealing, with 100 °C annealing for 20 minutes and with 140 °C annealing for

20 minutes. All the annealing was done in the glovebox, as the PTB7 molecules are not air stable. Then $5nm$ of calcium and $100nm$ of aluminium were be deposited on the samples as top electrodes. The evaporation was be performed at 10^{-7}Torr to ensure proper deposition. The filtering of the active layer was difficult, With the application of force some of the liquid turned foamy and passed through.Visible aggregation could be seen on the samples.
The second and third batch the only differed in the way we treated the samples and equipment prior to the spincoating of the active layer. We decided to bring the heat up to 80 °C and stir for several hours. We heated up the PTB7, PDI solutions prior to mixing, and the equipment (needle, syringe, filter) and the samples prior to the spincoating up to 80 °C for 15 minutes. We then spun the samples as quickly as possible after taking the required instruments off the hotplate. We observed a remarkable improvement in the film quality, and the filtration went a lot better.

4.4 Standard deviation calculation

We have calculated the root mean square deviation in the measurements, and because we took a limited amount of measurements we used:

$$RMSD = \sqrt{\frac{1}{N-1}\sum_{i=1}^{N}(x_i - \overline{x})^2}$$

where N is the sample size, x_i is the i^{th} measurement of parameter X, and $\overline{x}$ is the average value of x

Bibliography

[1] Tai-Sang Ahn, Astrid M Müller, Rabih O Al-Kaysi, Frank C Spano, Joseph E Norton, David Beljonne, Jean-Luc Brédas, and Christopher J Bardeen. Experimental and theoretical study of temperature dependent exciton delocalization and relaxation in anthracene thin films. *The Journal of chemical physics*, 128(5):054505, 2008.

[2] YV Aulin. *Singlet Exciton Fission and Photochemical Upconversion*. PhD thesis, TU Delft, Delft University of Technology, 2016.

[3] Carl J Ballhausen. Ligand field theory. 1962.

[4] William Barford. *Electronic and optical properties of conjugated polymers*. Number 129. Oxford University Press, 2005.

[5] D Beljonne, Z Shuai, G Pourtois, and JL Bredas. Spin-orbit coupling and intersystem crossing in conjugated polymers: A configuration interaction description. *The Journal of Physical Chemistry A*, 105(15):3899–3907, 2001.

[6] Timothy C Berkelbach, Mark S Hybertsen, and David R Reichman. Microscopic theory of singlet exciton fission. i. general formulation. *The Journal of chemical physics*, 138(11):114102, 2013.

[7] JB Birks, JH Appleyard, and Rosalind Pope. The photo-dtmers of anthracene, tetracene and pentacene. *Photochemistry and Photobiology*, 2(4):493–495, 1963.

[8] John Betteley Birks. *Organic molecular photophysics*, volume 2. John Wiley & Sons, 1975.

[9] Mordechai Bixon and Joshua Jortner. Intramolecular radiationless transitions. *The Journal of Chemical Physics*, 48(2):715–726, 1968.

[10] Jean-Luc Brédas, David Beljonne, Veaceslav Coropceanu, and Jérôme Cornil. Charge-transfer and energy-transfer processes in π-conjugated oligomers and polymers: a molecular picture. *Chemical Reviews*, 104(11):4971–5004, 2004.

[11] Richard H Bube. Photoconductivity. *Wiley Encyclopedia of Electrical and Electronics Engineering*, 1960.

[12] J Burgos, M Pope, Ch E Swenberg, and RR Alfano. Heterofission in pentacene-doped tetracene single crystals. *physica status solidi (b)*, 83(1):249–256, 1977.

[13] Wai-Lun Chan, Manuel Ligges, and XY Zhu. The energy barrier in singlet fission can be overcome through coherent coupling and entropic gain. *Nature chemistry*, 4(10):840–845, 2012.

[14] J Clark, T Nelson, S Tretiak, G Cirmi, and G Lanzani. Femtosecond torsional relaxation. *Nature Physics*, 8(3):225–231, 2012.

[15] Tracey M Clarke and James R Durrant. Charge photogeneration in organic solar cells. *Chemical reviews*, 110(11):6736–6767, 2010.

[16] Daniel N Congreve, Jiye Lee, Nicholas J Thompson, Eric Hontz, Shane R Yost, Philip D Reusswig, Matthias E Bahlke, Sebastian Reineke, Troy Van Voorhis, and Marc A Baldo. External quantum efficiency above 100% in a singlet-exciton-fission–based organic photovoltaic cell. *Science*, 340(6130):334–337, 2013.

[17] Janke J Dittmer, Elisabeth A Marseglia, and Richard H Friend. Electron trapping in dye/polymer blend photovoltaic cells. *Advanced Materials*, 12(17):1270–1274, 2000.

[18] Samuel W Eaton, Leah E Shoer, Steven D Karlen, Scott M Dyar, Eric A Margulies, Brad S Veldkamp, Charusheela Ramanan, Daniel A Hartzler, Sergei Savikhin, Tobin J Marks, et al. Singlet exciton fission in polycrystalline thin films of a slip-stacked perylenediimide. *Journal of the American Chemical Society*, 135(39):14701–14712, 2013.

[19] William E Ford and Prashant V Kamat. Photochemistry of 3, 4, 9, 10-perylenetetracarboxylic dianhydride dyes. 3. singlet and triplet excited-state properties of the bis (2, 5-di-tert-butylphenyl) imide derivative. *Journal of Physical Chemistry*, 91(25):6373–6380, 1987.

[20] Stephen R Forrest. The path to ubiquitous and low-cost organic electronic appliances on plastic. *Nature*, 428(6986):911–918, 2004.

[21] Christoph Gadermaier, G Cerullo, G Sansone, G Leising, U Scherf, and G Lanzani. Time-resolved charge carrier generation from higher lying excited states in conjugated polymers. *Physical review letters*, 89(11):117402, 2002.

[22] N Geacintov, M Pope, and F Vogel. Effect of magnetic field on the fluorescence of tetracene crystals: exciton fission. *Physical Review Letters*, 22(12):593, 1969.

[23] NE Geacintov, M Pope, and S Fox. Magnetic field effects on photo-enhanced currents in organic crystals. *Journal of Physics and Chemistry of Solids*, 31(6):1375–1379, 1970.

[24] Andrew Gilbert and James Edward Baggott. *Essentials of molecular photochemistry*. CRC, 1991.

[25] Natalie Gorczak, Marcel Swart, and Ferdinand C Grozema. Energetics of charges in organic semiconductors and at organic donor–acceptor interfaces. *Journal of Materials Chemistry C*, 2(17):3467–3475, 2014.

[26] Eric C Greyson, Brian R Stepp, Xudong Chen, Andrew F Schwerin, Irina Paci, Millicent B Smith, Akin Akdag, Justin C Johnson, Arthur J Nozik, Josef Michl, et al. Singlet exciton fission for solar cell applications: Energy aspects of interchromophore coupling†. *The Journal of Physical Chemistry B*, 114(45):14223–14232, 2009.

[27] RP Groff, P Avakian, and RE Merrifield. Coexistence of exciton fission and fusion in tetracene crystals. *Physical Review B*, 1(2):815, 1970.

[28] Jiamo Guo, Hideo Ohkita, Hiroaki Benten, and Shinzaburo Ito. Near-ir femtosecond transient absorption spectroscopy of ultrafast polaron and triplet exciton formation in polythiophene films with different regioregularities. *Journal of the American Chemical Society*, 131(46):16869–16880, 2009.

[29] E Hädicke and F Graser. Structures of eleven perylene-3, 4: 9, 10-bis (dicarboximide) pigments. *Acta Crystallographica Section C: Crystal Structure Communications*, 42(2):189–195, 1986.

[30] Roald Hoffmann. An extended hückel theory. i. hydrocarbons. *The Journal of Chemical Physics*, 39(6):1397–1412, 1963.

[31] Ian A Howard, Frederic Laquai, Panagiotis E Keivanidis, Richard H Friend, and Neil C Greenham. Perylene tetracarboxydiimide as an electron acceptor in organic solar cells: a study of charge generation and recombination. *The Journal of Physical Chemistry C*, 113(50):21225–21232, 2009.

[32] Chun Huang, Stephen Barlow, and Seth R Marder. Perylene-3, 4, 9, 10-tetracarboxylic acid diimides: Synthesis, physical properties, and use in organic electronics. *The Journal of organic chemistry*, 76(8):2386–2407, 2011.

[33] Erich Hückel. Zur quantentheorie der doppelbindung. *Zeitschrift für Physik*, 60(7-8):423–456, 1930.

[34] Klaus Hunger. *Industrial dyes: chemistry, properties, applications*. John Wiley & Sons, 2007.

[35] Lijun Huo, Yi Zhou, and Yongfang Li. Synthesis and absorption spectra of n-type conjugated polymers based on perylene diimide. *Macromolecular Rapid Communications*, 29(17):1444–1448, 2008.

[36] Priya J Jadhav, Patrick R Brown, Nicholas Thompson, Benjamin Wunsch, Aseema Mohanty, Shane R Yost, Eric Hontz, Troy Van Voorhis, Moungi G Bawendi, Vladimir Bulović, et al. Triplet exciton dissociation in singlet exciton fission photovoltaics. *Advanced Materials*, 24(46):6169–6174, 2012.

[37] Justin C Johnson, Arthur J Nozik, and Josef Michl. High triplet yield from singlet fission in a thin film of 1, 3-diphenylisobenzofuran. *Journal of the American Chemical Society*, 132(46):16302–16303, 2010.

[38] Brooks A Jones, Michael J Ahrens, Myung-Han Yoon, Antonio Facchetti, Tobin J Marks, and Michael R Wasielewski. High-mobility air-stable n-type semiconductors with processing versatility: Dicyanoperylene-3, 4: 9, 10-bis (dicarboximides). *Angewandte Chemie*, 116(46):6523–6526, 2004.

[39] William Jorgensen. *The organic chemist's book of orbitals*. Elsevier, 2012.

[40] Michael Kasha. Characterization of electronic transitions in complex molecules. *Discussions of the Faraday society*, 9:14–19, 1950.

[41] Peter M Kazmaier and Roald Hoffmann. A theoretical study of crystallochromy. quantum interference effects in the spectra of perylene pigments. *Journal of the American Chemical Society*, 116(21):9684–9691, 1994.

[42] G Klein, R Voltz, and M Schott. Magnetic field effect on prompt fluorescence in anthracene: evidence for singlet exciton fission. *Chemical Physics Letters*, 16(2):340–344, 1972.

[43] G Klein, R Voltz, and M Schott. On singlet exciton fission in anthracene and tetracene at 77° k. *Chemical Physics Letters*, 19(3):391–394, 1973.

[44] A Köhler and H Bässler. Triplet states in organic semiconductors. *Materials Science and Engineering: R: Reports*, 66(4):71–109, 2009.

[45] Anna Köhler and David Beljonne. The singlet–triplet exchange energy in conjugated polymers. *Advanced Functional Materials*, 14(1):11–18, 2004.

[46] Tim Kowalczyk, Shane R Yost, and Troy Van Voorhis. Assessment of the δscf density functional theory approach for electronic excitations in organic dyes. *The Journal of chemical physics*, 134(5):054128, 2011.

[47] Heinz Langhals. Cyclic carboxylic imide structures as structure elements of high stability. novel developments in perylene dye chemistry. *Heterocycles*, 1(40):477–500, 1995.

[48] Heinz Langhals, Jan Karolin, and Lennart B-Å Johansson. Spectroscopic properties of new and convenient standards for measuring fluorescence quantum yields. *Journal of the Chemical Society, Faraday Transactions*, 94(19):2919–2922, 1998.

[49] Ningning Liang, Kai Sun, Zhong Zheng, Huifeng Yao, Guangpeng Gao, Xiangyi Meng, Zhaohui Wang, Wei Ma, and Jianhui Hou. Perylene diimide trimers based bulk heterojunction organic solar cells with efficiency over 7%. *Advanced Energy Materials*, 2016.

[50] EC Lim, Joseph D Laposa, and MH Jack. Temperature dependence of intersystem crossing in substituted anthracenes. *Journal of Molecular Spectroscopy*, 19(1):412–420, 1966.

[51] Sang-Hyun Lim, Thomas G Bjorklund, Frank C Spano, and Christopher J Bardeen. Exciton delocalization and superradiance in tetracene thin films and nanoaggregates. *Physical review letters*, 92(10):107402, 2004.

[52] Michael P Marder. *Condensed matter physics*. John Wiley & Sons, 2010.

[53] RE Merrifield. Theory of magnetic field effects on the mutual annihilation of triplet excitons. *The Journal of Chemical Physics*, 48(9):4318–4319, 1968.

[54] RE Merrifield. Magnetic effects on triplet exciton interactions. *Pure and Applied Chemistry*, 27(3):481–498, 1971.

[55] Fatemeh Mirjani, Nicolas Renaud, Natalie Gorczak, and Ferdinand C Grozema. Theoretical investigation of singlet fission in molecular dimers: the role of charge transfer states and quantum interference. *The Journal of Physical Chemistry C*, 118(26):14192–14199, 2014.

[56] Yukie Mori, Yoshio Sakaguchi, and Hisaharu Hayashi. Spin effects on decay dynamics of charge-separated states generated by photoinduced electron transfer in zinc porphyrin-naphthalenediimide dyads. *The Journal of Physical Chemistry A*, 106(18):4453–4467, 2002.

[57] Andrew J Musser, Matz Liebel, Christoph Schnedermann, Torsten Wende, Tom B Kehoe, Akshay Rao, and Philipp Kukura. Evidence for conical intersection dynamics mediating ultrafast singlet exciton fission. *Nature Physics*, 11(4):352–357, 2015.

[58] Yukinori Nagao. Synthesis and properties of perylene pigments. *Progress in organic coatings*, 31(1):43–49, 1997.

[59] Jun-ichi Nakamura, Chiho Yokoe, Kazuhiko Murata, and Kohshin Takahashi. Efficient organic solar cells by penetration of conjugated polymers into perylene pigments. *Journal of applied physics*, 96(11):6878–6883, 2004.

[60] Alfred Pochettino. Sul comportamento fotoelettrico dell'antracene. *Acad. Lincei Rend*, 15:355, 1906.

[61] M Pope and CE Swenberg. Electronic processes in organic molecular crystals. *Oxford University Press, New York Tang CW, VanSlyke SA (1987) Organic electroluminescent diodes. Appl Phys Lett*, 51(913):89–103, 1982.

[62] Martin Pope and Charles E Swenberg. *Electronic processes in organic crystals and polymers*. Oxford University Press on Demand, 1999.

[63] Alfred G Redfield. On the theory of relaxation processes. *IBM Journal of Research and Development*, 1(1):19–31, 1957.

[64] Nicolas Renaud and Ferdinand C Grozema. Intermolecular vibrational modes speed up singlet fission in perylenediimide crystals. *The journal of physical chemistry letters*, 6(3):360–365, 2015.

[65] Nicolas Renaud, Paul A Sherratt, and Mark A Ratner. Mapping the relation between stacking geometries and singlet fission yield in a class of organic crystals. *The journal of physical chemistry letters*, 4(7):1065–1069, 2013.

[66] Armin Richter, Martin Hermle, and Stefan W Glunz. Reassessment of the limiting efficiency for crystalline silicon solar cells. *Photovoltaics, IEEE Journal of*, 3(4):1184–1191, 2013.

[67] Mahin Sadrai, Linda Hadel, Ronald R Sauers, Syeda Husain, Karsten Krogh-Jespersen, John D Westbrook, and George R Bird. Lasing action in a family of perylene derivatives: singlet absorption and emission spectra, triplet absorption and oxygen quenching constants, and molecular mechanics and semiempirical molecular orbital calculations. *The Journal of Physical Chemistry*, 96(20):7988–7996, 1992.

[68] Joel N Schrauben, Joseph L Ryerson, Josef Michl, and Justin C Johnson. Mechanism of singlet fission in thin films of 1, 3-diphenylisobenzofuran. *Journal of the American Chemical Society*, 136(20):7363–7373, 2014.

[69] Markus Schwoerer and Hans Christoph Wolf. *Organic molecular solids*. John Wiley & Sons, 2007.

[70] Jason M Serin, Darryl W Brousmiche, and Jean MJ Fréchet. Cascade energy transfer in a conformationally mobile multichromophoric dendrimer. *Chemical Communications*, (22):2605–2607, 2002.

[71] Boris Isaakovich Shklovskii and Alex L Efros. *Electronic properties of doped semiconductors*, volume 45. Springer Science & Business Media, 2013.

[72] William Shockley and Hans J Queisser. Detailed balance limit of efficiency of p-n junction solar cells. *Journal of applied physics*, 32(3):510–519, 1961.

[73] S Singh, WJ Jones, W Siebrand, BP Stoicheff, and WG Schneider. Laser generation of excitons and fluorescence in anthracene crystals. *The Journal of Chemical Physics*, 42(1):330–342, 1965.

[74] Millicent B Smith and Josef Michl. Singlet fission. *Chemical reviews*, 110(11):6891–6936, 2010.

[75] David W Snoke. *Solid state physics: Essential concepts*. Addison-Wesley, 2009.

[76] Corien W Struijk, Alexander B Sieval, Jarno EJ Dakhorst, Marinus van Dijk, Peter Kimkes, Rob BM Koehorst, Harry Donker, Tjeerd J Schaafsma, Stephen J Picken, Anick M van de Craats, et al. Liquid crystalline perylene diimides: architecture and charge carrier mobilities. *Journal of the American Chemical Society*, 122(45):11057–11066, 2000.

[77] CE Swenberg and WT Stacy. Bimolecular radiationless transitions in crystalline tetracene. *Chemical Physics Letters*, 2(5):327–328, 1968.

[78] Verner K Thorsmølle, Richard D Averitt, Jure Demsar, DL Smith, S Tretiak, RL Martin, X Chi, BK Crone, AP Ramirez, and AJ Taylor. Morphology effectively controls singlet-triplet exciton relaxation and charge transport in organic semiconductors. *Physical Review Letters*, 102(1):017401, 2009.

[79] Y Tomkiewicz, RP Groff, and P Avakian. Spectroscopic approach to energetics of exciton fission and fusion in tetracene crystals. *Journal of Chemical Physics*, 54:4504–4507, 1971.

[80] Linjun Wang, Yoann Olivier, Oleg V Prezhdo, and David Beljonne. Maximizing singlet fission by intermolecular packing. *The journal of physical chemistry letters*, 5(19):3345–3353, 2014.

[81] Michael R Wasielewski. Self-assembly strategies for integrating light harvesting and charge separation in artificial photosynthetic systems. *Accounts of chemical research*, 42(12):1910–1921, 2009.

[82] Tanja Weil, Tom Vosch, Johan Hofkens, Kalina Peneva, and Klaus Müllen. The rylene colorant family—tailored nanoemitters for photonics research and applications. *Angewandte Chemie International Edition*, 49(48):9068–9093, 2010.

[83] Tony C Wu, Nicholas J Thompson, Daniel N Congreve, Eric Hontz, Shane R Yost, Troy Van Voorhis, and Marc A Baldo. Singlet fission efficiency in tetracene-based organic solar cells. *Applied Physics Letters*, 104(19):193901, 2014.

[84] Frank Würthner. Perylene bisimide dyes as versatile building blocks for functional supramolecular architectures. *Chemical communications*, (14):1564–1579, 2004.

[85] Yu Zhong, Bharat Kumar, Seokjoon Oh, M Tuan Trinh, Ying Wu, Katherine Elbert, Panpan Li, Xiaoyang Zhu, Shengxiong Xiao, Fay Ng, et al. Helical ribbons for molecular electronics. *Journal of the American Chemical Society*, 136(22):8122–8130, 2014.

[86] Yu Zhong, M Tuan Trinh, Rongsheng Chen, Wei Wang, Petr P Khlyabich, Bharat Kumar, Qizhi Xu, Chang-Yong Nam, Matthew Y Sfeir, Charles Black, et al. Efficient organic solar cells with helical perylene diimide electron acceptors. *Journal of the American Chemical Society*, 136(43):15215–15221, 2014.

[87] P Zugenmaier, J Duff, and TL Bluhm. Crystal and molecular structures of six differently with halogen substituted bis (benzylimido) perylene. *Crystal Research and Technology*, 35(9):1095–1115, 2000.